Structure-based design of highly selective 2,4,5-trisubstituted pyrimidine CDK9 inhibitors as anti-cancer agents

Hao Shao,[a,1] David W. Foley,[a,1] Shiliang Huang,[a] Abdullahi Y. Abbas,[a, d] Frankie Lam,[b] Pavel Gershkovich,[a] Tracey D. Bradshaw,[a] Chris Pepper,[c] Peter M. Fischer,[a,*] Shudong Wang[a, b,*]

[a] School of Pharmacy and Biodiscovery Institute, University of Nottingham, University Park, Nottingham NG7 2RD, UK.

[b] Drug Discovery and Development, Clinical and Health Sciences, University of South Australia, Adelaide, SA 5001, Australia.

[c] Brighton and Sussex Medical School, University of Sussex, Brighton, East Sussex, BN1 9PX.

[d] Department of Biochemistry, Usmanu Danfodiyo University Sokoto, Nigeria, 840001

Corresponding Author

* Shudong Wang, E-mail: shudong.wang@unisa.edu.au, Clinical and Health Sciences, University of South Australia, Adelaide SA 5001, Australia. Tel.: +61 883022372; fax: +61 883021087.

* Peter M. Fischer, E-mail: peter.fischer@nottingham.ac.uk

1 co-first authors

Key words: RNA polymerase II; CDK9 inhibitor; apoptosis; Mcl-1; chronic lymphocytic leukaemia; anti-cancer agents

Abstract

Cyclin-dependent kinases (CDKs) are a family of Ser/Thr kinases involved in cell cycle and transcriptional regulation. CDK9 regulates transcriptional elongation and this unique property has made it a potential target for several diseases. Due to the conserved ATP binding site, designing selective CDK9 inhibitors has been challenging. Here we report our continued efforts in the optimization of 2,4,5-tri-substituted pyrimidine compounds as potent and selective CDK9 inhibitors. The most selective compound **30m** was > 100-fold selective for CDK9 over CDK1 and CDK2. These compounds showed broad anti-proliferative activities in various solid tumour cell lines and patient-derived chronic lymphocytic leukaemia (CLL) cells. Decreased phosphorylation of the carboxyl terminal domain (CTD) of RNAPII at Ser-2 and down-regulation of anti-apoptotic protein Mcl-1 were confirmed in both the ovarian cancer model A2780 and patient-derived CLL cells.

1. Introduction

Mammalian cells possess 21 cyclin-dependent kinases (CDKs) that fulfil major roles in cell cycle and transcription regulation.[1] CDKs1, 2, 4 and 6 are required to facilitate cell cycle progression. CDKs 8, 9, 12 and 19 are involved in the regulation of transcription through phosphorylation of the C-terminus of RNA polymerase II, while CDK7 is involved in both processes, [2, 3] CDK9 plays no clearly defined role in cell-cycle regulation but promotes transcription elongation. After initiation of RNA transcription, positive transcription elongation factor b (P-TEFb), consisting of cyclinT-CDK9, first phosphorylates the SpT5 (p160) subunit of DRB-sensitivity-inducing factor (DSIF) and the RD subunit of negative elongation factor (NELF) to remove promoter-proximal pausing on the transcription initiation complex. Subsequent phosphorylation of Ser2, and occasionally Ser5, on the carboxyl terminal domain (CTD) heptapeptide repeat of the largest subunit of RNAPII, promotes productive elongation.[4-8]

Constitutive expression of anti-apoptotic proteins is necessary for cancer cell's survival, which requires continuous activity of RNAPII. Mcl-1, an anti-apoptotic protein belonging to the Bcl-2 family, is highly expressed in numerous tumour cells in comparison with normal cells.[9, 10] It has been reported that the inhibition of Mcl-1 is sufficient to promote apoptosis in acute myeloid leukaemia (AML) and CLL cells [11, 12] and to overcome the resistance that cancer cells acquire upon treatment with Bcl-2 inhibitors.[13] Inhibition of CDK9 can abrogate the production of short-lived mRNA transcripts with anti-apoptotic functions and their corresponding proteins, thus leading to apoptosis of cancer cells.[4] Selective CDK9 inhibitors could therefore be used as either a single agent or in combination therapy. Indeed, multiple CDK9 inhibitors have shown efficacy in both solid tumors and haematological cancers.[14, 15] The CDK9 inhibitors voruciclib and A-1592668 can potentiate the anti-cancer efficacy of the Bcl-2 inhibitor ABT-199.[16, 17] We

also reported that an orally bioavailable CDK9 inhibitor CDKI-73 is active as a single agent in CLL [18], acute lymphoblastic leukaemia (ALL), AML [19], and colorectal cancer models [20]. In addition, CDKI-73 synergized with fludarabine in CLL [18], Bcl-2 inhibitor ABT-199 and BET inhibitor I-BET 151 in ALL and AML [21, 22], and PARP inhibitor olaparib in BRCA1 wide-type ovarian cancer [23].

Due to the therapeutic potential of CDK9 inhibition in cancer, tremendous efforts have been devoted to the CDK9 targeted drug discoveries.[15, 24] Flavopiridol was the first CDK inhibitor tested in clinical trials and the mechanistic studies showed that it achieved its efficacy mainly through potent inhibition of CDK9 in CLL.[25] More non-selective CDK9 inhibitors have since been discovered and are currently in various preclinical and clinical stages of development, summarized in a recent review.[15] In the past few years, selective CDK9 inhibitors such as NVP-2[26], JSH-150 [27], AZD5473 [28] and compound 30i [29] have been reported. Our and other studies showed that the selectivity for CDK9 can be achieved through modification of the substituents located at the hydrophobic channel adjacent to solvent.[27, 30, 31] In addition to this position, we gained CDK9 selectivity through modifying the substituents located at the hydrophobic pocket behind the gatekeeper residue. In this manuscript, we report our continued efforts in the design, synthesis and biological evaluation of 2,4,5-trisubstituted pyrimidine compounds as potent and selective CDK9 inhibitors.

## 2. Results and discussions

2.1. Chemistry
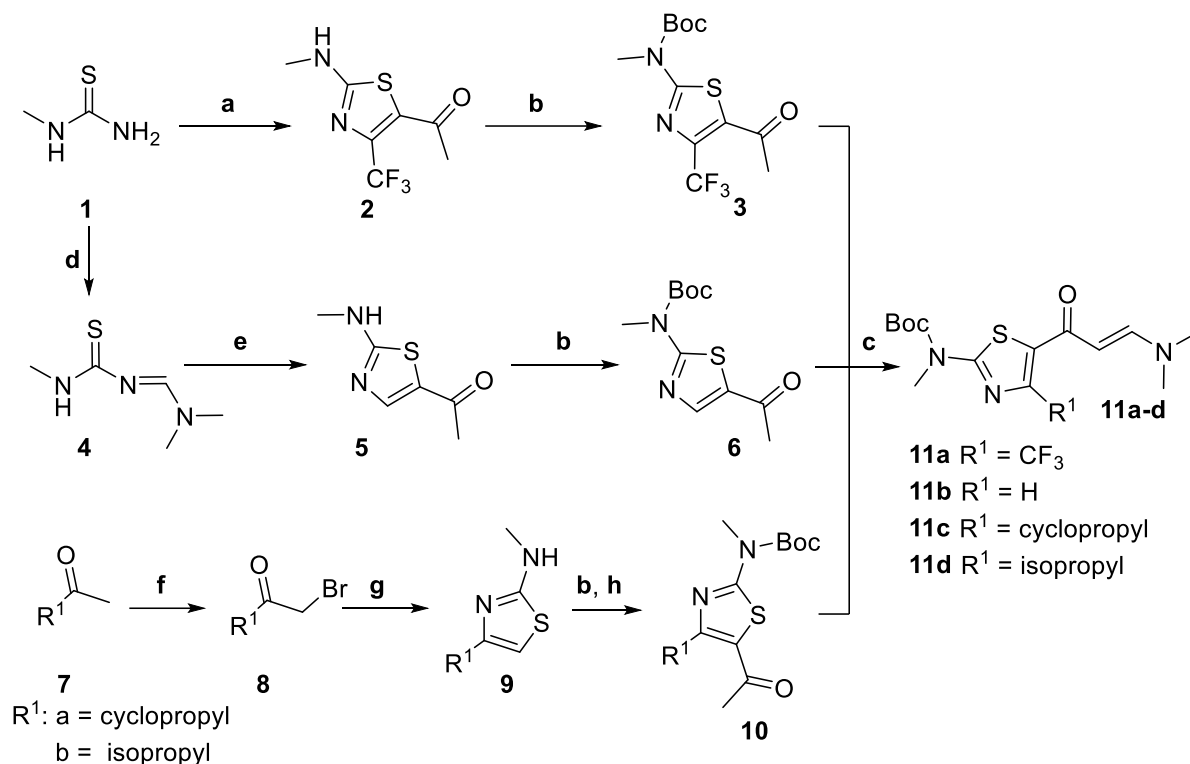
Scheme 1 Reagents and conditions: (a) *i.* 1,1,1-trifluoropentane-2,4-dione, hydroxy(tosyloxy)iodobenzene, MeCN, Δ, 1 h; *ii.* **1**, Δ, 4 h, 53 %; (b) Boc₂O, DMAP, CH₂Cl₂, RT, 2 h, 95%; (c) DMF-DMA, Δ, overnight or microwave radiation, 30 min-1 h, 77-92%. (d) DMF-DMA, CHCl₃, RT, overnight, 98%; (e) CH₃COCH₂Cl, MeCN, Δ, 4 h, 79%; (f) Br₂, MeOH, 0 °C to rt 4 h, 76-77%; (g) **1**, Δ, 4 h, 50-53 %; (h) *i.* Acetaldehyde, LDA, THF, -78 °C, 2 h; *ii.* MnO₂, CHCl₃, RT, 4 h, 65-85%.

Enaminones **11a-d** were synthesized using the methods previously reported, which are shown in

Scheme 1. Briefly, 1,1,1-trifluoropentane-2,4-dione was treated with hydroxy-(tosyloxy)iodobenzene, followed by reaction with 1-methylthiourea **1** to obtain thiazole **2**.

Condensation of methyl-thiourea **1** with DMF-DMA yielded **4** [32] followed by thiazole ring formation by cyclization with chloroacetone to afford 5-acetyl-4-hydrogen thiazole **5**.[33] 5-Acetyl thiazoles **2** and **4** were Boc protected then converted to the corresponding enaminones **11a-b** using standard conditions. α-bromoketones **8** were formed from the corresponding ketones using bromine and then condensed with 1-methylthiourea **1** to afford the 5-*H* thiazoles **9**, after Boc

protection. **9** was deprotonated with LDA and reacted with acetaldehyde to form the alcohols, which were oxidized to ketones **10** using manganese dioxide.[34]
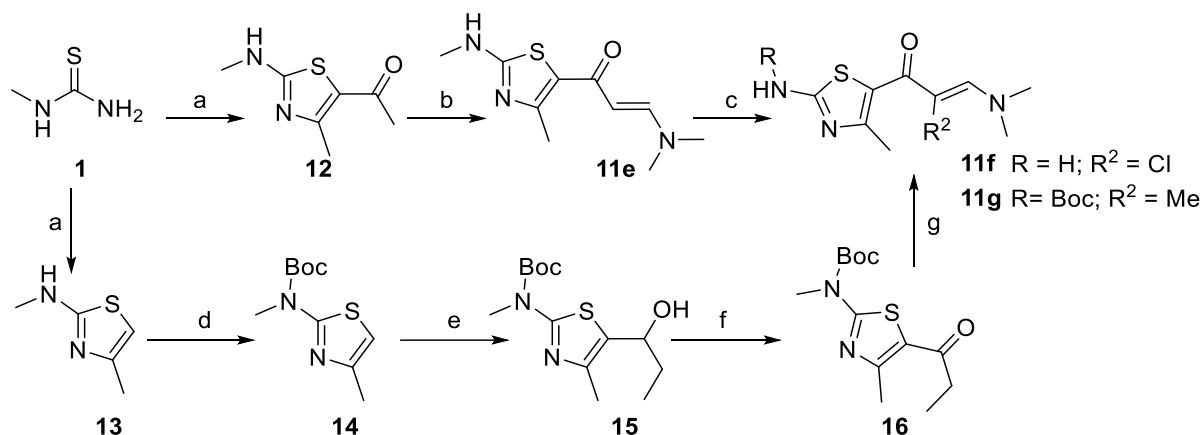

Scheme 2 Reagents and conditions: (a) 3-chloro-2,4-pentadione, pyridine, EtOH, RT, 4 h, 98%; (b) DMF-DMA, Δ, MeCN, overnight, 90%; (c) NCS, MeOH, 0 °C, 2 h, 60%; (d) Boc₂O, DMAP, CH₂Cl₂, room temp, 2 h; (e) propionaldehyde, LDA, THF, -78 °C, 2 h; (f) MnO₂, CHCl₃, RT, 4 h, 65-85%; (g) DMF-DMA, microwave radiation, 30 min-1 h.

Scheme 2 shows the synthesis of the enaminone **11f** and **11g**. The synthesis of enaminone **11f** started from 1-methylthiourea **1**, which was cyclized with 3-chloro-2,4-pentadione to yield 5-acetyl thiazole **12**.[35] **12** was then treated with DMF-DMA to form the corresponding enaminone **11e**, which was converted to chlorine substituted enaminone **11f** using *N*-chlorosuccinimide in moderate yields. 1-Methylthiourea **1** was treated with chloroacetone to afford the thiazole **13**. After Boc protection, compound **14** was deprotonated with LDA and reacted with propionaldehyde to form the alcohol **15**. Ketone **16** was formed by oxidation using manganese dioxide. Enaminone **11g** was synthesized using a microwave method and in the next step without purification.
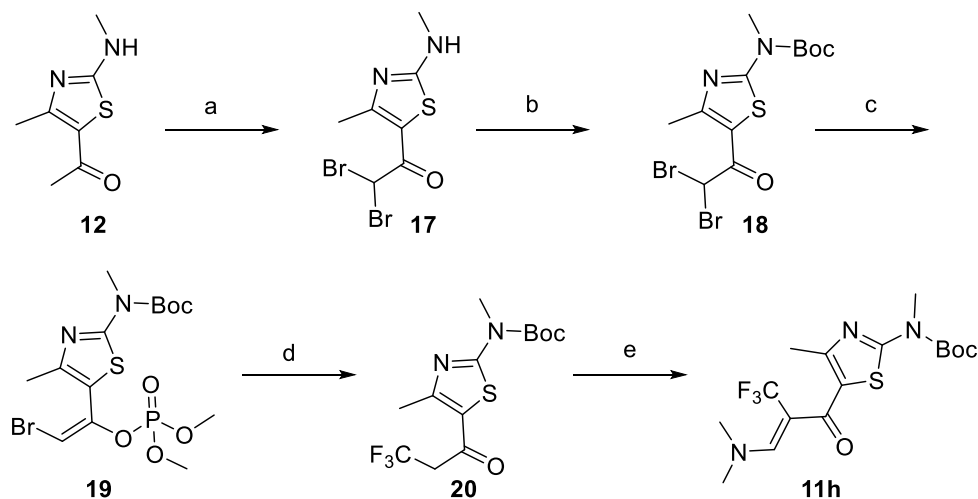
Scheme 3: Reagents and conditions: (a) Br$_2$, 48% HBr solution, 60 °C, 3 h, 56 %; (b) Boc$_2$O, DMAP, CH$_2$Cl$_2$, RT, 2 h; (c) trimethylphosphite, RT, 22 h; (d) FO$_2$SCF$_2$CO$_2$CH$_3$, CuI/DMF, 80 °C, overnight, 37 % over 3 steps; (e) DMA-DMA, Δ, 1 h, 64 %.

The synthesis of enaminone **11h** is outlined in **Scheme 3**. Thiazole **12** was treated with two equivalents of a 48% solution of bromine in HBr to obtain the dibromo compound **17**.[36] After Boc protection, β-bromoenol phosphate **19** was obtained following a Perkow reaction. Treatment of **19** with methyl 2,2-difluoro-2-(fluorosulfonyl)acetate in the presence of CuI led to the formation of the desired trifluoromethylated intermediate **20**. The enaminone **11h** was then synthesized using the standard conditions.
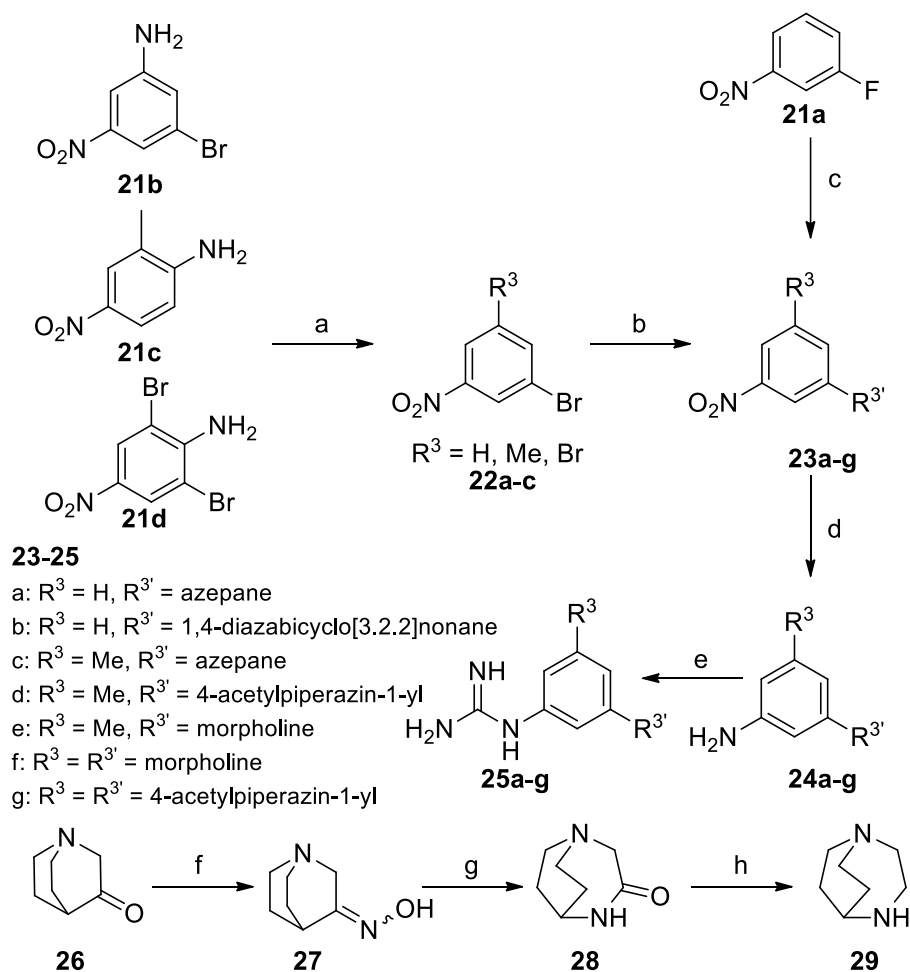
Scheme 4: Reagents and conditions: (a): H_2SO_4, $NaNO_2$, EtOH, Δ, 3 h, 69%-89%; (b): $Pd_2(dba)_3$, (+/-)-BINAP, Cs_2CO_3, Dioxane, 90 °C, 5d, 16%-89%; (c): amines, DMSO, 100 °C, 72 h, 53-77%; (d): RaNi, $NH_2NH_2 \cdot H_2O$, 0 °C, 30 min-1 h or H_2, Pd/C, EtOH: EtOAc 1:1, overnight, 90%-96%; (e): NH_2CN, TMSCl, ACN, Δ, 6 h or microwave, 100-140 °C, 20−45 min, 35%-78%; (f): $NH_2OH \cdot HCl$, $C_2H_3NaO_2$, H_2O, Δ, 90 min, 65%; (g): H_3PO_4, 120-140 °C, slow addition of 37 over 2 h, 38%; (h): $LiAlH_4$, dioxane, Δ, 6h, 83%.

The synthesis of the guanidine intermediates is summarised in **Scheme 4**. Mono-substituted guanidines were synthesized as previously described *via* nucleophilic aromatic substitution (NAS) of fluoro-nitrobenezene **21a**.[35] For di-substituted guanidines the corresponding NAS approach was not successful, so Buchwald coupling of **22b-d** was employed. The nitro group was then reduced and reacted with cyanamide as previously described. The amines employed were readily commercially available, with the exception of the bicyclic amine 1,4-diazabicyclo[3.2.2]nonane

29, which was synthesized *via* a Beckmann rearrangement and reduction of the commercially available quinuclidin-3-one **26**.
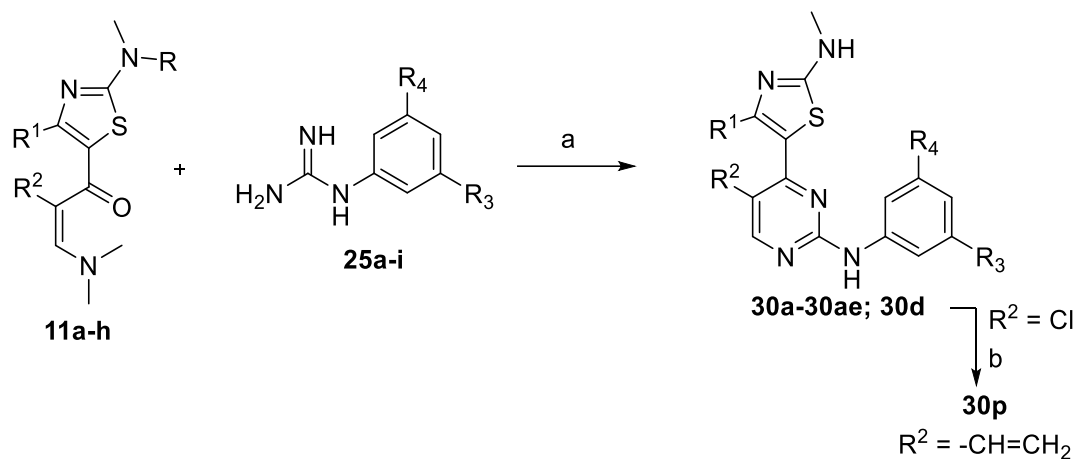
Scheme 5 Reagents and conditions. (a) 2-methoxyethanol, microwave, 100-140 °C, 20−45 min; (b) (tributylstannyl)ethylene, 3% Pd[(t-Bu)$_3$P]$_2$, CsF, 1,4-dioxone, microwave, 120 °C, 2 h, 60%.

Finally, the component parts of the final compounds were combined in a condensation reaction using microwave conditions as previously reported and summarized in **Scheme 5**.[30] A Stille coupling was used to introduce a vinyl substituent in place of a chlorine at the C5-position of the pyrimidine, as shown in **Scheme 5**.
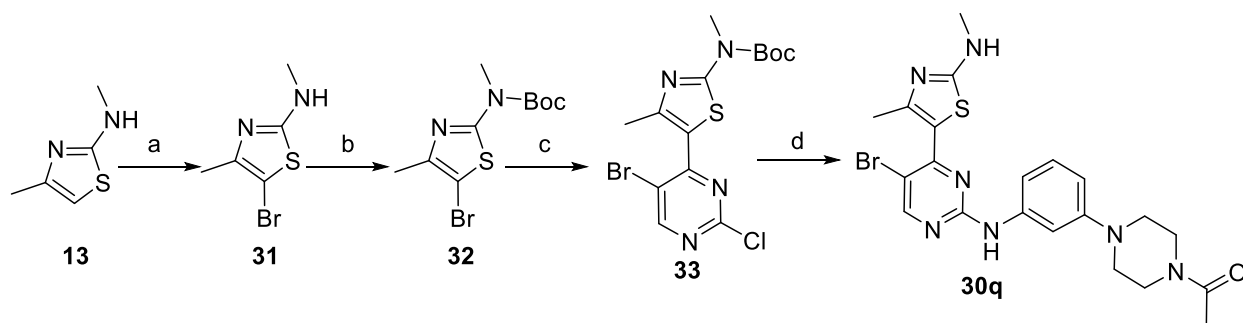
Scheme 6: Reagents and conditions: (a) NBS, AcOH, RT, 2 h, 88 % (crude); (b) Boc$_2$O, DMAP, CHCl$_3$, RT, 2 h, 60 %; (c) *i*. LDA, -78 °C, 30 min; *ii*. 5-bromo-2-chloropyrimidine, -78 °C, 1 h; *iii*. AcOH, DDQ in THF; 77 %; (d) 3-(4-acetyl-1-piperazinyl)aniline, 2-methoxyethanol, microwave radiation, 140 °C, 45 min, 28 %.

The introduction of a bromo substituent into the 5-position of the pyrimidine differs from the previous synthetic method and is summarized in **Scheme 6**. Briefly, the thiazole **13** was brominated using *N*-bromosuccinimide in acetic acid to afford **31**. After Boc protection of the amine, compound **32** was treated with butyl lithium for 30 minutes and then 5-bromo-2-chloropyrimidine. After completion of the reaction, it was quenched with acetic acid and DDQ was added to yield compound **33**. The final compound **30q** was synthesized by treating compound **33** with 3-(4-acetyl-1-piperazinyl)aniline.

2.2. Ligand design, structure-activity relationships and molecular docking

We have previously reported 2,4,5-trisubstituted pyrimidine compounds as potent CDK9 inhibitors but selectivity for CDK9 over CDK2 remained a challenge.[30, 31] We elected to rationally design inhibitors with improved selectivity for CDK9 by taking advantage of the structural differences between CDK2 and CDK9. By comparing the amino acid residues that form the active site of CDK2 and CDK9, we hoped to identify non-conserved regions that could be targeted with suitably designed compounds.[37] Although CDK2 and CDK9 share the same phenylalanine gatekeeper residue, differences in the hydrophobic pocket behind the gatekeeper residue have been successfully exploited to generate selective CDK4 and CDK7 inhibitors.[38, 39] In the hydrophobic channel adjacent to solvent, residues are less conserved. For example, CDK9 has a non-ionisable side chain in the Lys89 (positively charged) position of CDK2, and the electrostatic charge differences of the hydrophobic channel can be used for improving the CDK9 selectivity.[40] In addition, the region around Ala111-Gly112 in CDK9 is much more open than the corresponding Lys88-Lys89 region in CDK2 due to differences in size between alanine, glycine and lysine. This pocket in CDK9 is therefore both larger and more hydrophobic than

CDK2, both features that could be exploited for selectivity.[40, 41] Residues around this region among CDKs are less conserved and have been used for optimizing selectivity.

Several hypotheses were proposed to enable the design of highly selective CDK9 inhibitors based on the differences discussed above: (i) Co-crystal structures of the lead compound **30a** bound to CDK2 revealed that the C-4 methyl of the thiazole was packed up against the Phe80 gatekeeper residue (Fig. 1).[35] Modification of this R^1 substituent may therefore dramatically change the kinase inhibition profile; (ii) R^2 could be extended into the hydrophobic pocket to form favorable interactions with the gatekeeper residue Phe103 of CDK9, evidenced by compound **30b** (Fig. 1). In addition, the introduction of substituents at this position induces a steric clash with the R^1 substituent on the thiazole ring. This causes a twist in the conformation of the molecule when compared to the observed co-planarity of the thiazole and pyrimidine rings in a co-crystal structure of **30a** with CDK2.[35] Additionally, the steric clash induced by substitution on both the thiazole and pyrimidine rings could induce an even greater twist of these two ring systems than that observed in the crystal structures. This would dramatically alter the conformation of the molecule and could therefore adjust the SAR. (iii) Various R^3 substituents with different sizes and electronic properties could be introduced to the molecule to optimise the kinase potency and selectivity, as well as exploring tolerance for future optimization of physicochemical properties.
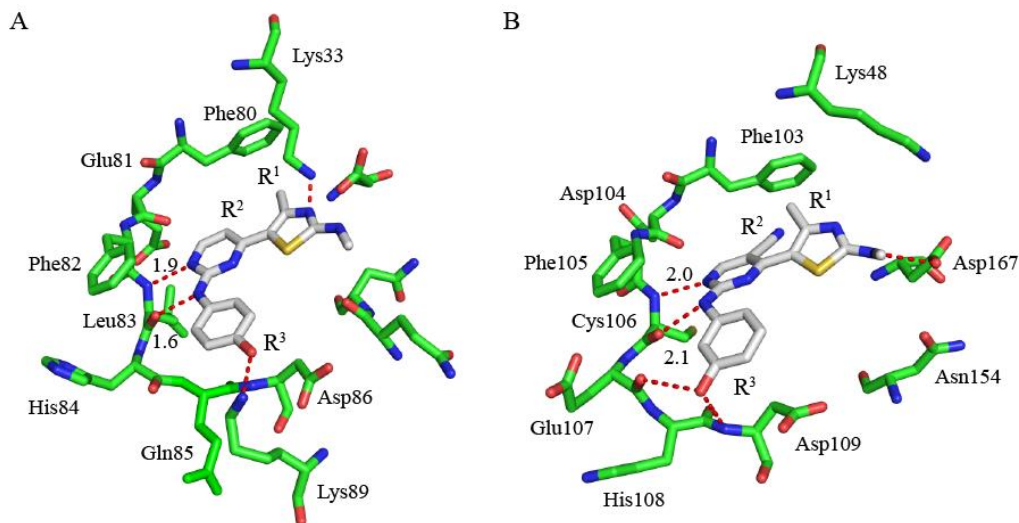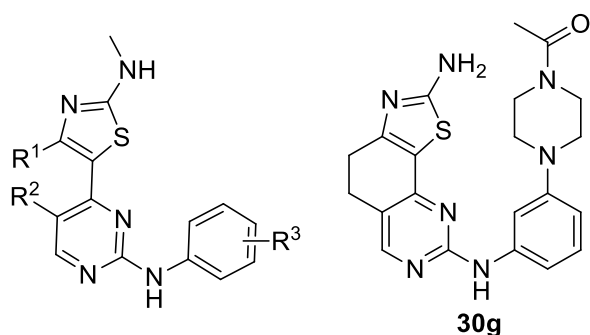
Fig. 1. Binding poses of lead compounds **30a** and **30b** within CDK2 and CDK9: (a) Crystal structure of **30a** bound to CDK2 (PDB code 1PXN); (b) Crystal structure of **30b** bound to CDK9 (PDB code 4BCJ). Selected CDK2 and CDK9 residues are drawn in stick representation and the carbons of CDK2/9 are green. The carbons of **30a** and **30b** are grey. Hydrogen bonds are depicted by dotted red lines. The images were generated by Pymol.

Based on these rationales, we synthesized a series of compounds and their structure activity relationships (SAR) are summarized in Table 1. Compound **30c**, containing chlorine at the C-5 position of the pyrimidine ring, was a low nanomolar potent CDK9 inhibitor and showed ~21-fold selectivity for CDK9 over CDK2. When the methylpiperazine of R^3 was changed to morpholine, compound **30d** showed comparable CDK9 potency with compound **30c** and the CDK9/CDK2 selectivity dropped to 5-fold. Both of these compounds were potent against HCT-116 and MCF-7 cell lines with GI_{50} values of ~0.5 µM.

Table 1: Structure activity relationships

Compd	Structure			K_i (nM)[a]		SI[c]	GI$_{50}$ (μM)[b]	
	R^1	R^2	R^3	CDK9T1	CDK2A		HCT-116	MCF-7
30a	Me	H	*p*-OH	-	70	-	-	-
30b	Me	CN	*m*-OH	11	12	1	0.03 ± 0.005	0.07 ± 0.01
30c	Me	Cl	*m*-methylpiperazine	5	107	21	0.66 ± 0.06	0.68 ± 0.11
30d	Me	Cl	*m*-morpholine	4	22	6	0.43 ± 0.08	0.72 ± 0.03
30e	Me	Me	*m*-morpholine	10	444	44	0.36 ± 0.11	0.45 ± 0.20
30f	Me	Me	*m*-4-acetylpiperazin-1-yl	12	794	66	0.55 ± 0.01	3.65 ± 0.37
30g	-	-	-	34	87	2.5	0.06 ± 0.02	0.08 ± 0.02
30h	Me	Me	*m*-piperazine	8	711	89	0.83 ± 0.04	0.86 ± 0.05
30i	Me	Me	*m*-methylpiperazine	20	586	29	1.29 ± 0.16	1.89 ± 0.25
30j	Me	Me	*m*-4-(methylsulfonyl)piperazine	7	87	12	0.50 ± 0.05	0.83 ± 0.18
30k	Me	Me	*m*-1,4-diazepane	8	1244	156	1.37 ± 0.70	0.87 ± 0.15
30l	Me	Me	*m*-1,4-diazepan-5-one	19	525	28	2.12 ± 0.58	6.44 ± 0.26
30m	Me	Me	*m*-1,4-diazabicyclo[3.2.2]nonane	10	1248	125	1.07 ± 0.04	1.34 ± 0.28
30n	Me	CF$_3$	*m*-4-acetylpiperazin-1-yl	95	1223	13	4.80 ± 0.14	25.0 ± 3.96
30o	Me	CF$_3$	*m*-piperazine	49	1934	40	4.05 ± 0.21	3.05 ± 0.35
30p	Me	vinyl	*m*-morpholine	62	503.5	8	> 5	> 5

30q	Me	Br	*m*-4-acetylpiperazin-1-yl	7.5	125	16	-	-
30r	CF$_3$	H	*m*-1,4-diazepane	8	14	2	0.07 ± 0.01	0.65 ± 0.01
30s	H	H	*m*-1,4-diazepane	3	22	7	0.08 ± 0.004	0.06 ± 0.01
30t	cycloprop	H	*m*-CO-*N*-(1-methylpiperidin-4-yl)	40	128	3	0.77 ± 0.01	1.95 ± 0.02
30u	isopro	H	*m*-4-acetylpiperazin-1-yl	91	680	8	0.08 ± 0.01	0.07 ± 0.01
30v	Me	H	*m*-4-acetylpiperazin-1-yl	32	281	9	0.58 ± 0.08	5.28 ± 0.25

[a]The data given are mean values derived from two replicates of one experiment. Apparent inhibition constants (K_i) were calculated from IC$_{50}$ values and the appropriate K_m (ATP) values for each kinase; [b]Anti-proliferative activity by MTT-48 h assay; the data given are mean values derived from at least three independent replicates, internal repeats n=3; [c]SI represents selectivity index ($K_{i, CDK2}$/ $K_{i, CDK9}$).

Keeping the morpholine moiety, but replacing the C-5 chlorine with a methyl substituent, affords compound **30e**, which significantly enhanced the CDK9/CDK2 selectivity to 44-fold. A further improvement of CDK9/CDK2 selectivity was obtained by replacing the morphine moiety with 4-acetyl-piperazine. Selectivity was completely abolished when **30f** was ring constrained into the bridged analog **30g** or when the C-5 methyl was replaced by hydrogen (**30v**), which supports our hypotheses that inducing a twist between the pyrimidine and thiazole rings could be exploited to improve selectivity. In **30g**, molecular modelling suggested that the thiazole and pyrimidine rings were coplanar because of the restricted rotation, whereas the clash of the methyl groups in **30f** resulted in a twist of the two rings, generating a non-planer conformation (**Fig. 2**). It is possible that this conformational change drives the selectivity between CDK9 and CDK2, and that CDK9 can better accommodate the non-planer conformation due to the greater flexibility of its binding pocket.
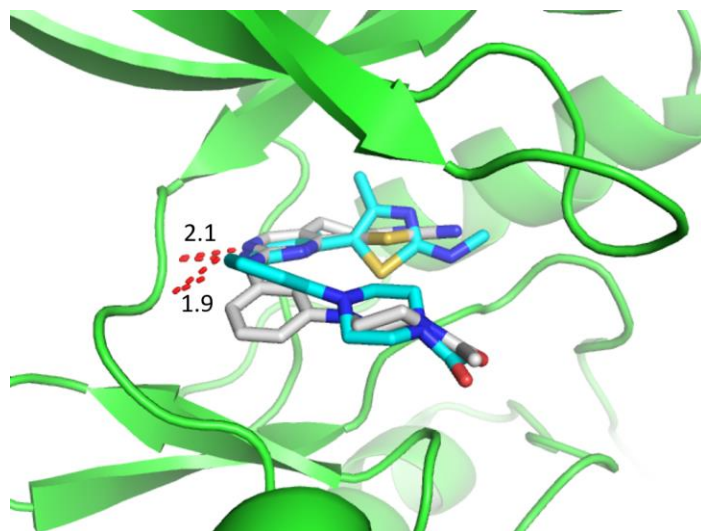
Fig. 2. Overlay of compound **30f** and **30g** docked with CDK9 (PDB ID 4BCG). The kinase is presented in green in cartoon representation. Carbon atoms of **30f** and **30g** are grey and cyan respectively. Hydrogen bonds are denoted by red dashed lines. The images were generated by Pymol.

The kinase selectivity profile varied greatly in the C5-methyl series of compounds when there were minor changes in the R^3 substituents. The piperazine analog **30h** gave the best selectivity between CDK9 and CDK2 among the six membered-ring analogs, ~90-fold. Methylation of the piperazine resulted in **30i**, which decreased the K_i to 20 nM and the CDK9/CDK2 selectivity decreased from 88-fold to 28-fold. The methylsulfonyl piperazine analog **30j** did not change the CDK9 potency, but the CDK9/CDK2 selectivity was only ~12-fold. These analogs showed variable cellular potency, with GI_{50} values from 0.36-0.86 μM in the two cancer lines. The CDK9/CDK2 selectivity was reduced when the NH was replaced with an O (**30e**), acetylated (**30f**), methylated (**30i**) or converted to the sulfonamide (**30j**), suggesting that a hydrogen bond donor or a positively charged moiety in this position was critical for selectivity.

Introduction of the bulkier 7-membered 1,4-diazepane ring at the R^3 position led to the most selective compounds in this series, exemplified by compound **30k**, which showed ~156-fold selectivity for CDK9 over CDK2. Yet again, disrupting the hydrogen bond donor ability of the 1,4-diazepane by conversion to the lactam **30l** greatly reduced selectivity. Bridged diazepane

analog **30m** maintained the selectivity for CDK9 over CDK2, ~120-fold. There was little change in the cellular potencies of selective compounds compared to non-selective compounds (*cf* **30m** and **30d**). This suggested that inhibition of CDK9 also contributed to the observed anti-cancer activity to a large extent.

To rationalize the selectivity of **30k** and **30m**, we docked the molecules into active sites of the models generated from the crystal structures 4BCG (CDK9) and 4BCP (CDK2) using a rigid protein docking method as discussed previously. 3**0k** was predicted to bind to CDK9 and CDK2 in a similar manner to the observed crystallographic binding mode of the inherent ligand (**Fig. 3A** and **B**). The *meta*-anilino substituent of **30k** was bound differently in CDK9 and CDK2. In the CDK9/cyclinT/**30k** complex (**Fig. 3A**), the 1,4-diazepane moiety was positioned towards the thiazole ring, adjacent to the ribose position of ATP in the kinase structures, which we termed as an 'inward' conformation. By contrast, in the CDK2/cyclinA/**30k** complex, this moiety was positioned away from the thiazole and directed towards the hinge region (**Fig. 3B**), which was termed the 'outward' conformation.

However, when we attempted this docking with **30m**, it became clear that it could not be accommodated by the CDK9 model generated from 4BCG. As the protein structure was rigid during the docking process, the bridged diazepane was too bulky to fit in the pocket. We therefore attempted to dock **30m** into receptors generated from alternative crystal structures of CDK9 [4BCF] and CDK2 [4BCO]. In this case, compound **30m** showed a similar binding pose to compound **30k** in CDK9 (**Fig. 3C**). A clash between the methyl substituent of the thiazole ring with CDK2 was observed (**Fig. 3D**). When the two sets of CDK9 crystal structures (4BCG and 4BCF) were overlaid, the difference is the position of the glycine-rich loop and it is possible that the ligand binding pocket became smaller because of the downward movement of the glycine-rich

loop in 4BCG compared to 4BCF. For proteins as flexible as CDK9, rigid docking platforms may not be the best approach for computational modelling and experiments should therefore be performed on various examples of reported crystal structures to overcome this limitation.
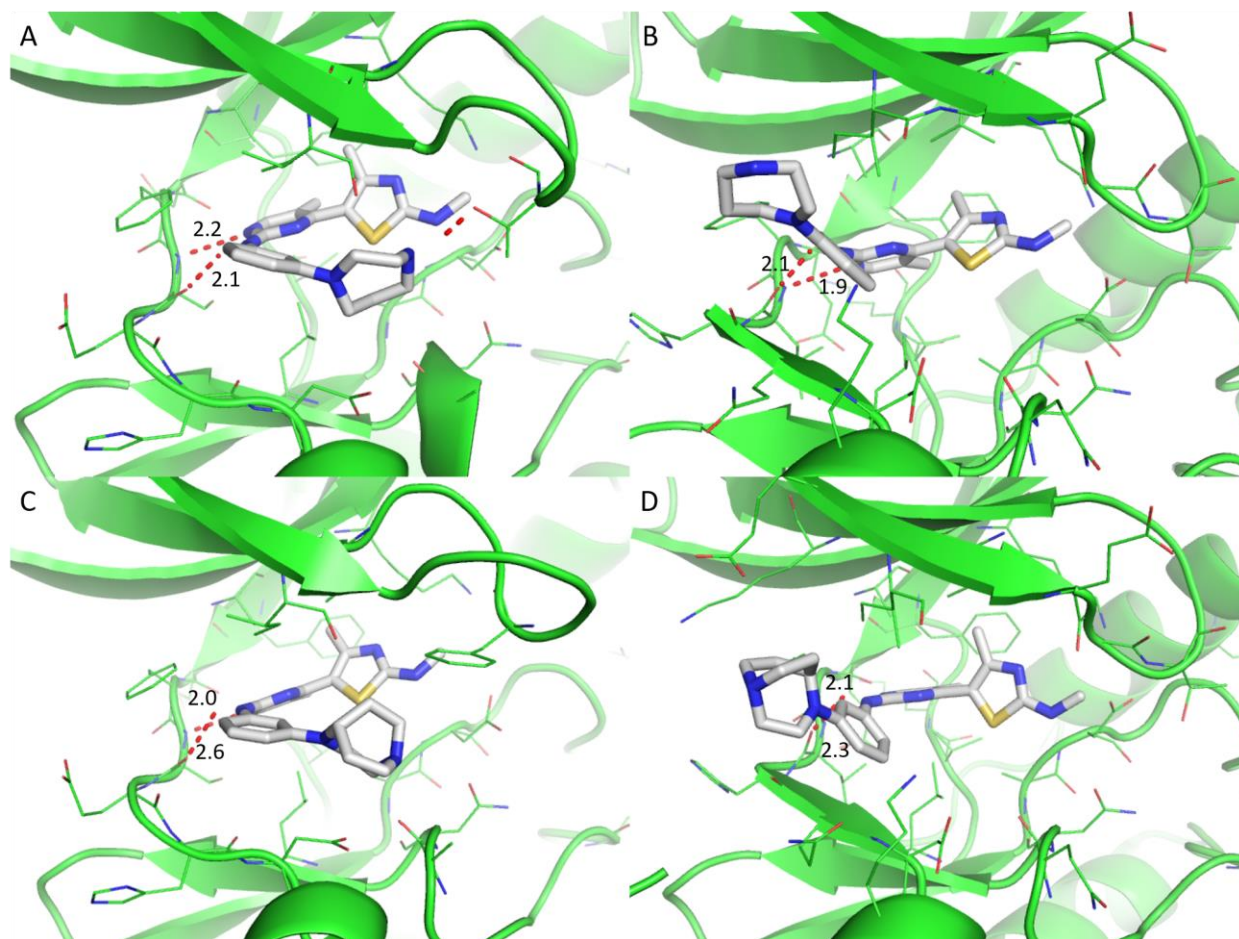

Fig. 3. Docking poses for complexes of CDK9 and CDK2 with compound **30k** and **30m**. (**A**): CDK9/**30k,** model generated from PDB 4BCG; (**B**): CDK2/**30k,** model generated from PDB 4BCP; (**C**): CDK9/**30m**, model generated from 4BCF; (**D**): CDK2/**30m**, model generated from 4BCO. The kinase is presented in green in cartoon representation and selected residues are drawn in lines mode. Carbon atoms of **30k** and **30m** are grey and hydrogen bonds are denoted by red dashed lines. The images were generated by Pymol.

Methyl groups have been frequently replaced by trifluoromethyl groups as bioisosteres in medicinal chemistry. The trifluoromethyl group is generally more metabolically stable than the

methyl group because of the strong C-F bond and has also been used for improving oral bioavailability.[42, 43] The trifluoromethyl group is also a strong electron-withdrawing group and may help to improve the hinge region binding between ligand and protein. Therefore, the corresponding C-5 trifluoromethyl pyrimidine analogs were synthesized. Compounds **30n** and **30o** were 10-40-fold selective towards CDK9 over CDK2, but lost potency against both kinases and cells compared with its C-5 methyl analogs **30f** and **30h**. These two trifluoromethyl analogs had GI_{50} against two human cell lines ranging from 3.05-25.0 µM. A study of van der Waals volumes of trifluoromethyl and various alkyl groups has suggested that a trifluoromethyl group has a similar size to an ethyl group, but their shapes are different.[44, 45] Given that our previous SAR showed that a C-5 ethyl pyrimidine analog lost both CDK9 and CDK2 potency,[30] we believe this steric effect explains why the trifluoromethyl group was not tolerated. This is further supported by the fact that a vinyl substituent in this position (**30p**) was also not tolerated. The C-5 bromo pyrimidine analog **30q** showed comparable CDK9/CDK2 selectivity (16-fold) to its chlorine analog **30c**.

From the above SAR, it can be concluded that both the steric and electronic properties of substituents at the C-5 position of the pyrimidine ring affect the potency and selectivity of kinase inhibition. The C-5 chloro, bromo and methyl pyrimidine analogs have different selectivity profiles presumably because of their different electronic properties, considering their similar size. It was clear from the above SAR that the introduction of a methyl group at the C-5 of the pyrimidine ring was optimal for achieving selectivity for CDK9.

After exploring the SAR of R^2 position, we turned our attention to the R^1 position of the thiazole ring to further probe the gatekeeper pocket. By keeping six- or seven-membered rings at the R^3 position on the aniline ring, compounds **30r-30v** with various R^1 substituents were synthesized to interrogate SAR. The kinase potency and cellular activity of compounds with small R^1 groups

(**30r,** R^1 = CF$_3$, and **30s,** R^1 = H) was improved and selectivity for CDK9 over CDK2 was lost. When the bulk at R^1 was increased to a cyclopropyl unit, both potency and selectivity (compound **30t**) were decreased. An isopropyl analog **30u** also showed a loss in potency, although a similar selectivity profile to the corresponding methyl analog **30v** was observed. Interestingly, compound **30u** was much more potent against both cancer cells than **30v**, indicating potential off-target effects. In order to rationalize why compounds with R^1 as cyclopropyl and isopropyl substituents lost activities, molecular docking simulations were carried out. Compound **30t** and **30u** were docked into CDK9 (PDB code 4BCG) and the binding poses of the top 5 scores were visualized. No inward conformation was observed with compound **30t** in the top 5 docking poses and only one inward pose of compound **30u** was observed among the top 5 scores. More poses with the thiazole rings flipping about 180 degrees were observed, which may because the small hydrophobic pocket around the gatekeeper residue Phe103 was too small to accommodate the isopropyl and cyclopropyl substituents.

Our above SAR clearly indicated a trend between increasing the bulk of this 7-membered ring still further and improving CDK9 selectivity over CDK2. We therefore proposed that molecules containing bulky groups at both *meta* positions of the aniline would show preferential binding to CDK9, as these must place some bulk in the inward conformation by virtue of their di-substitution pattern. A series of such compounds was therefore synthesized (**30w**-**30ae**, **Table 2**). In general, bulky disubstituted anilines were more selective for CDK9 than CDK2, with compound **30ae** being 30-fold selective for CDK9 compared to 9-fold for **30v**. However, dramatic improvements to selectivity were not observed and no compound in this series approached the 100-fold selectivity window.

We proposed three hypotheses to improve the selectivity for CDK9 over other CDKs. Introducing substituents with various size and electronic properties at R^1 position did not change the selectivity profile, but affected compounds' potency against CDKs. Only by introducing a substituent at R^2 position, especially methyl group, dramatically improved the selectivity for CDK9 over other CDKs. This confirmed our hypothesis that a conformation change induced by the clash of R^1 and R^2 substituents is important for selectivity. Noticing that the pocket close to solvent exposed region was more open in CDK9 than CDK2, we designed and synthesized bulky mono- and di-substituted analogs. 7-membered 1,4-diazepane and bridged diazepane substituted analogs **30k** and **30m** achieved the best selectivity among this series. However, di-substituted analogs **30w**-**30ae** did not further improve the selectivity.

Table 2: Structure activity relationships
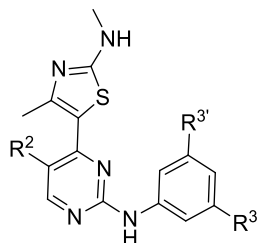
Compd	Structure			K_i (nM)[a]		SI[c]	GI$_{50}$ (µM)[b]	
	R^2	R^3	R^4	CDK9T1	CDK2A		HCT-116	MCF-7
30w	CN	H	azepane	6	44	7	1.54 ± 0.23	4.13 ± 0.81
30x	CN	Me	azepane	25	52	2	4.05 ± 0.49	7.04 ± 0.64
30y	CN	Me	piperazine	6	45	8	0.08 ± 0.01	0.61 ± 0.01
30z	CN	Me	morpholine	5	16	3	0.49 ± 0.07	0.95 ± 0.01
30aa	H	morpholine	morpholine	47	831	18	0.34 ± 0.08	0.38 ± 0.04
30ab	H	4-acetylpiperazin-1-yl	4-acetylpiperazin-1-yl	187	2074	11	0.20 ± 0.07	0.42 ± 0.07
30ac	CN	morpholine	morpholine	9	55	6	0.02 ± 0.001	0.09 ± 0.001
30ad	CN	4-acetylpiperazin-1-yl	4-acetylpiperazin-1-yl	21	248	12	0.70 ± 0.04	2.40 ± 0.57
30ae	Me	4-acetylpiperazin-1-yl	4-acetylpiperazin-1-yl	43	1369	32	0.78 ± 0.15	2.00 ± 0.35

[a]The data given are mean values derived from two replicates of one experiment. Apparent inhibition constants (K_i) were calculated from IC$_{50}$ values and the appropriate K_m (ATP) values for each kinase. [b]Anti-proliferative activity by MTT-48 h assay; the data given are mean values derived from at least three independent replicates ; [c]SI represents selectivity index ($K_{i, CDK2}/ K_{i, CDK9}$).

2.3. Diversity kinase panel screening

As **30h**, **30k** and **30m** showed good selectivity for CDK9 over CDK2, they were selected to test

against CDK1 and CDK7. All showed approximately 100-fold selectivity for CDK9 over CDK1.

30h and **30m** also showed a selectivity against CDK7 (> 50-fold), although only 10-fold selectivity

was achieved by **30k**. Compound **30m** was further tested against a diversity panel of 60 kinases at a concentration of 20 x CDK9 K_i (0.2 µM, **Fig. 4**). **30m** showed a good selectivity profile, only 5 other kinases (Aurora-A, MLK1, NEK2, KDR and Fyn) being potently inhibited.

Table 3: Structure and activity relationships

Compd	Kinase inhibition K_i (nM)[a]			
	CDK9T1	CDK2A	CDK1B	CDK7H
30h	8	711	1120	472
30k	8	1244	785	89
30m	10	1248	1170	546

[a]The data given are mean values derived from two replicates. Apparent inhibition constants (K_i) were calculated from IC$_{50}$ values and the appropriate K_m (ATP) values for each kinase.
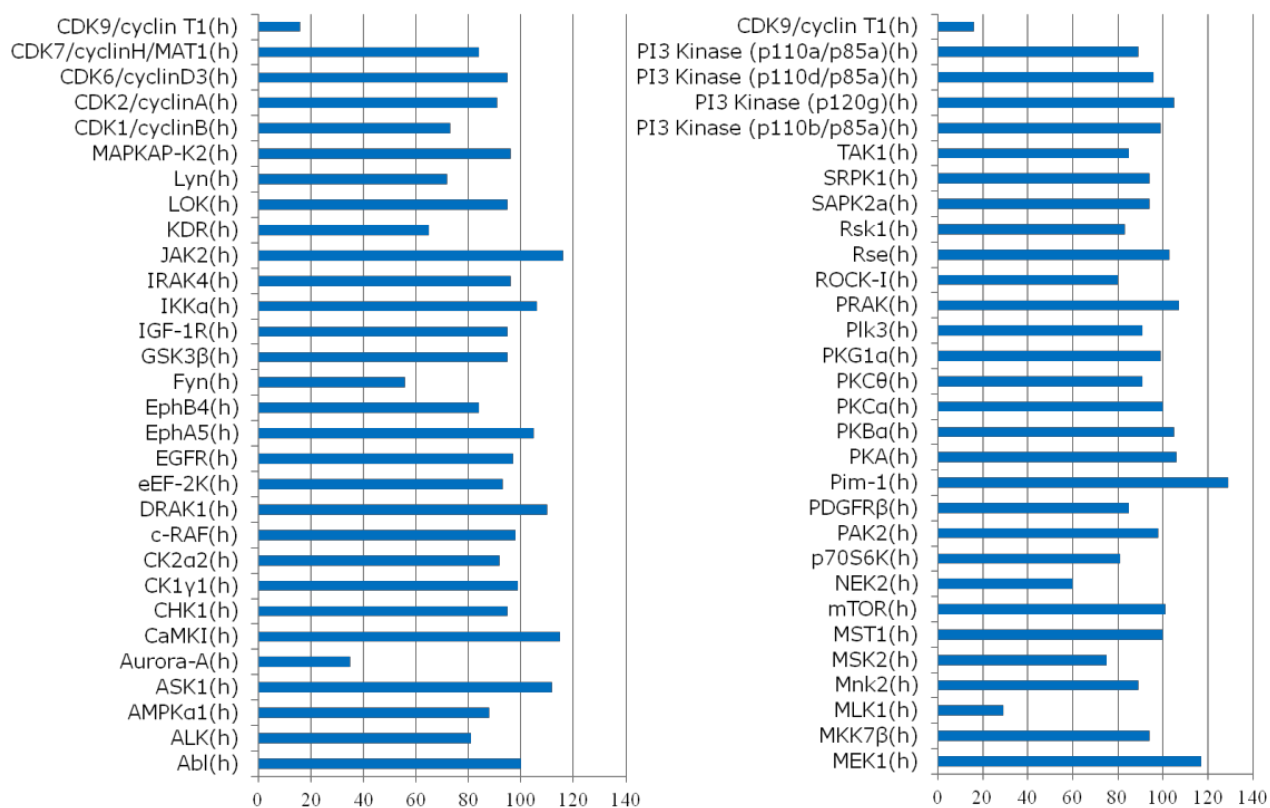
Fig. 4. Diversity kinase panel screening of **30m**. The assay was carried out in duplicate. Percentage of remaining kinase activity is shown.

2.4. Biological evaluation CDK9 inhibitors in cancer cells

30m was further evaluated for its mechanism of action in tumour cell lines and CLL patient-derived cells.

*2.4.1. **30m** showed broad anti-proliferative activities*

30m was found to be a potent anti-proliferative agent against a panel of human cancer cell lines, including cancer of the colon, breast, lung, ovary, cervix, and pancreas, with GI_{50} values ranging from 0.64-2.10 µM (**Table 4**). **30m** was 10-20 fold less potent than flavopiridol, likely due to its enhanced selectivity for CDK9 compared to flavopiridol.

Table 4: Anti-proliferative activity of **30m**

Tissue Origin	Cell Line	GI_{50} (µM) ± S.D. (48h MTT)	
		Flavopiridol	**30m**
Colon	HCT-116	0.056 ± 0.013	1.07 ± 0.04
	HT-29	0.131 ± 0.013	2.10 ± 0.45
Breast	MCF-7	0.092 ± 0.005	1.34 ± 0.28
	MDA-MB-468	0.096 ± 0.006	1.46 ± 0.58
Lung	A549	0.145 ± 0.006	1.54 ± 0.57
Ovary	A2780	0.064 ± 0.001	0.64 ± 0.06
Cervix	HeLa	0.043 ± 0.001	0.80 ± 0.15
Pancreas	Miacapa-2	0.078 ± 0.018	1.07 ± 0.13

*2.4.2. **30m** induced apoptosis of cancer cells*

Induction of apoptosis in the A2780 ovarian cancer cell line 24 h post treatment with **30m** was confirmed by Annexin V/PI assay (**Fig. 5**). **30m** increased the percentage of apoptotic populations following treatment with 1 μM **30m** (18%) and reaching to 26% and 67% at 2 μM and 5 μM, respectively, when compared to untreated cells.
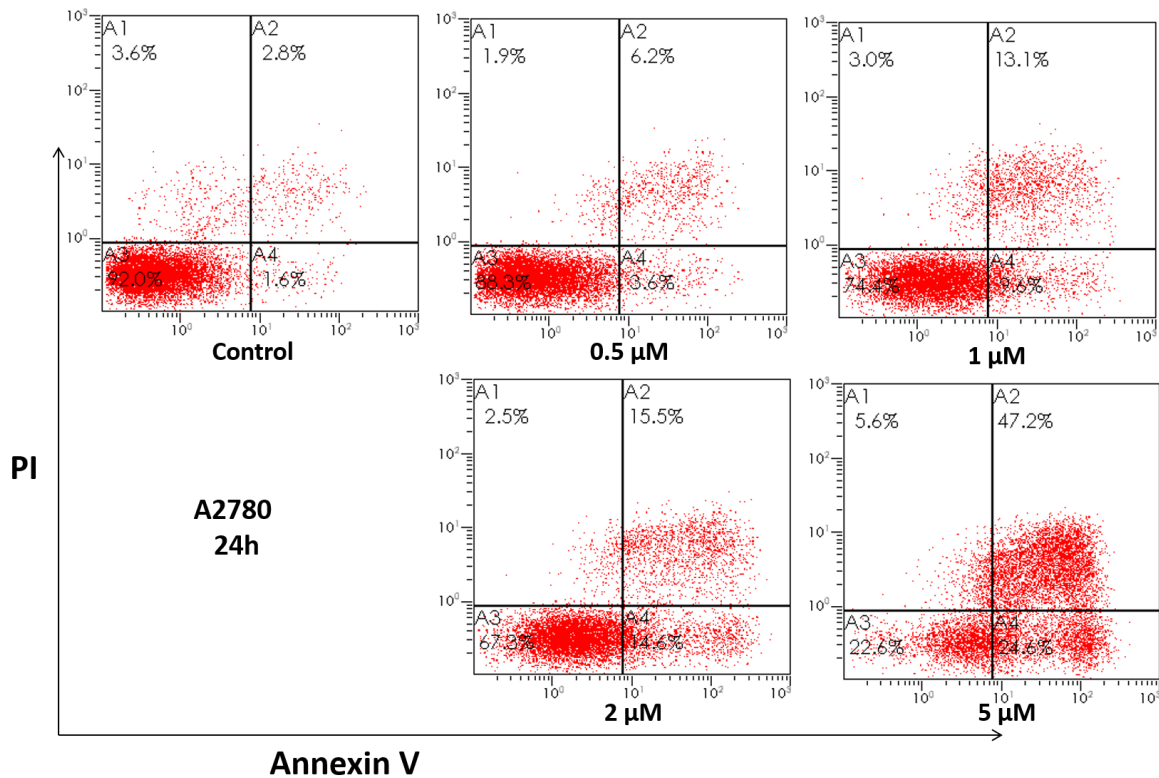

Fig. 5. Induction of apoptosis by **30m**. A2780 cells were treated with **30m** for 24 h at the concentrations shown and analyzed by annexin V/PI staining. Representative of three independent experiments is shown.

Caspase-3 is the effector caspase responsible for proteolytic cleavage of proteins involved in cell cycle regulation and DNA repair. Cell death induced by anti-cancer agents can occur through caspase-dependent or -independent mechanisms. To determine whether the cytotoxicity induced by **30m** is caspase-dependent, a caspase-3 fluorometric assay was performed. As shown in **Fig. 6**,

caspase-3 was activated in a dose-dependent manner with the highest activity at 5 µM compared to untreated controls.
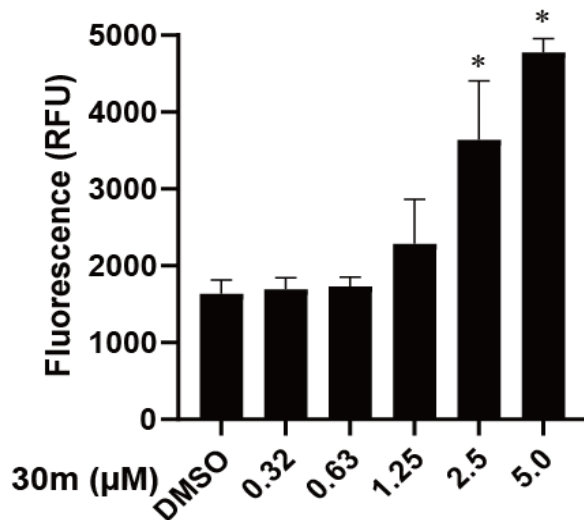

Fig. 6. Activation of caspase-3 in A2780 cancer cell line after treatment with **30m** for 24 h. Vertical bars represent the mean ± SD of two independent experiments, internal repeats n = 3. Values significantly ($P \leq 0.05$) different from DMSO diluent are marked with an asterisk (*).

2.4.3. *30m induced cell arrest in G2-M phase*

The effect of **30m** on cell cycle progression was investigated in A2780 cells. Cells were treated with increasing concentrations of **30m** for 24 h (**Fig. 7**). Accumulation of cells in the G2/M phase was detected at 1 and 2 µM of **30m**. A dose-dependent increase of cells in pre-G1 phase was observed, indicating cell death. The treatment with 5 µM of **30m** resulted in 34 % pre-G1 cells, which was consistent with the annexin V/PI staining assay.
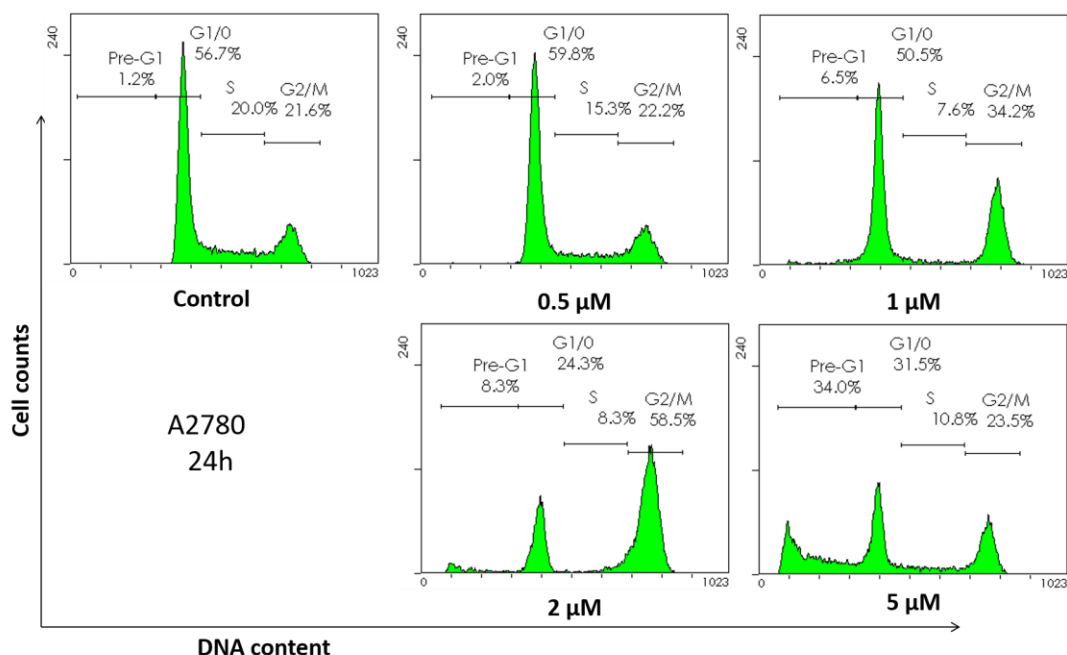
Fig. 7. Cell cycle effects of **30m**. A2780 cells were treated with **30m** for 24 h, followed by propidium iodide (PI) staining and analyzed by flow cytometry. Representative of three independent experiments is shown.

Inhibition of CDK1B and CDK2A can arrest the G2/M cell cycle. However, it is unlikely that the cell cycle effect is due to inhibition of CDK1B and 2A, as **30m** showed low activity against both kinases (K_i value of 1,248 and 1,170 nM, respectively, Table 3). Inhibition of CDK9 has been shown to block the G2/M cell cycle; for example, flavopiridol caused a shift from G0/G1 to G2/M phase in multiple cancer cells.[46] Another possible reason is the off-target effect, since **30m** inhibited aurora kinases A (**Fig. 4**), which has have a known role in regulation of the G2 to mitosis.

2.4.4. ***30m*** *inhibited phosphorylation of RNAPII CTD and down-regulated expression of anti-apoptotic proteins*

CDK9 regulates mRNA transcription by phosphorylation of the RNAPII at Ser-2 and Ser-5. Western blotting analysis of A2780 cancer cells 24 h-post treatment with **30m** showed that the

level of phosphorylated Ser-2 and Ser-5 was reduced by **30m** from ≥ 0.5 μM in a concentration-dependent manner, confirming cellular CDK9 inhibition of **30m** (**Fig. 8**).
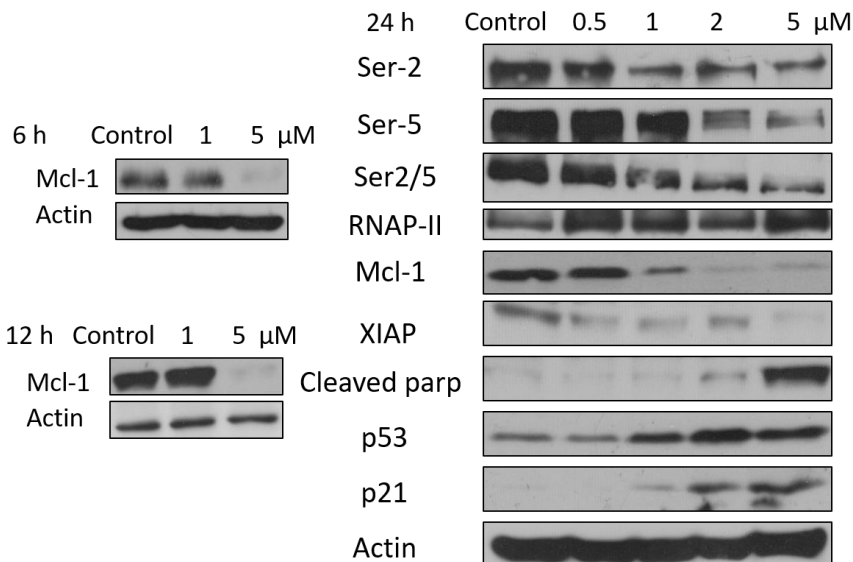

Fig. 8. Cellular mode of action of **30m**. A2780 cells were treated with **30m** and analyzed by Western blot. DMSO diluent was used as control in each experiment and β-actin antibody was used as an internal loading control.

Up-regulation of anti-apoptotic proteins, such as Mcl-1, Bcl-2 and XIAP, has been considered as the key mechanism of resistance to cancer therapies. Transcriptional inhibition of expression of Mcl-1 and XIAP is a general feature of CDK9 inhibitors. Consistently, treatment of A2780 cancer cells with **30m** for 6 or 12 h resulted in the down-regulation of Mcl-1 at 5 μM concentration (left panel, **Fig. 8**). The extended treatment for 24 h reduced the level of Mcl-1 and XIAP starting from 0.5 μM in a dose-dependent manner (right panel, **Fig. 8**), which was accompanied by PARP cleavage, confirming apoptosis. **30m** increased p53 levels and activated its transcriptional target gene, as evidenced by p21 induction. However, there was little difference in the GI_{50} values in the cell lines tested (**Table 4**), regardless of its p53 status, so wildtype p53 function is not required for **30m** to act. As in ovarian cancer cells, **30m** demonstrated a similar mode of action in HCT-

116 colorectal cancer cells (data not shown). We also demonstrated a similar mechanism of action to **30 m** of **30k** in the HCT-116 cell line (Supplemental data).

2.4.5. Ex vivo antitumor activity in primary CLL cells

30m, as well as **30k**, were further evaluated in patient-derived CLL cells using an annexin V-FITC apoptosis assay and the LD_{50} values are shown in **Table 5**. The potency of the two compounds seemed to be patient-dependent, since each patient had different clinical characteristics (Supplemental Table 2). **30k** was potent against most of patient-derived CLL cells except patient C with LD_{50} values ranging from 0.81 - 1.4 µM. Similarly, **30m** was potent against the cells derived from patients A-B and D-E with $LD_{50} = 1.5 – 6.2$ µM. The cells derived from patient C were found to be resistant to **30k** and **30m**. Patient C was in the early stage of CLL, and it is not clear why this disease was insensitive to both **30k** and **30m**. The cellular mode of action of **30k** and **30m** was confirmed in patient B derived cells where reduction of CDK9-mediated Mcl-1 expression leading to apoptosis was observed (Supplemental Fig. 5.).

Table 5. Cytotoxicity of **30k** and **30m** in CLL patient derived cells

Compd	$*LD_{50}$, µM				
	Patient A	Patient B	Patient C	Patient D	Patient E
30k	1.4	0.83	18	0.81	0.94
30m	6.2	2.3	82	1.5	2.9

* Concentration required to kill 50% of CLL cells following treatment for 48 h.

3. Conclusion

We have described the rational design, synthesis and biological evaluation of selective CDK9 inhibitors. Although the gatekeeper residue is conserved among CDKs, we found that this region

can be exploited to improve the selectivity for CDK9 over other members of CDK family. The selectivity for CDK9 over CDK2 and other kinases was improved greatly compared with the lead compound, evidenced by **30k** and **30m**. Our study provides important strategies for designing highly selective CDK9 inhibitors, which could also be applied to other kinase inhibitors as well.

Non-selective CDK9 inhibitors showed more potent cellular activity. As we improved the selectivity profile of the molecules, potency against CDK9 remained relatively similar. This suggests that our molecules have reduced off-target liabilities that are contributing to the cellular effects on non-selective compounds. Despite this, our lead molecules **30k** and **30m** retained potent anti-proliferative activity and a cellular mode of action consistent with a CDK9-targeted mechanism.

Since pan-selective CDKs inhibitors have not achieved clinical success, we suggest that this profile represents a significant improvement and that highly selective CDK9 inhibitors have potential to be developed as anti-cancer agents. This hypothesis must be further tested in preclinical study and clinical development.

4. Experimental section

4.1. Chemistry

Chemical reagents and solvents were obtained from commercial sources. When necessary, solvents were dried and/or purified by standard methods. ^{1}H-NMR and ^{13}C-NMR spectra were obtained using a Bruker 400, 500 or 600 Ultrashield™ spectrometer at 400, 500, 600 MHz and 100, 125, 150 MHz respectively. These were analyzed using the Bruker TOPSPIN 2.1 program. Chemical shifts are reported in parts per million relative to the solvent chemical shift. Coupling constants (*J*) are quoted to the nearest 0.1 Hz. The following abbreviations (or combinations thereof) are used: s, singlet; d, doublet; t, triplet; q, quartet; m, multiplet and br, broad. High

resolution mass spectra were obtained using a Waters 2795 single quadrupole mass spectrometer/micromass LCT platform. Purity for final compounds was greater than 95% and was measured using a Waters high performance liquid chromatography (Waters 2487 dual λ absorbance detector) with a Phenomenex Gemini-NX 5u C18 110A 250 × 4.60 mm column, UV detector at 254 nm, using system A: 10% MeOH containing 0.1% TFA for 4 min, followed by linear gradient 10 - 100% MeOH over 10 min at a flow rate of 1 mL/min; B: 10% MeOH containing 0.1% TFA for 4 min, followed by linear gradient 10 - 100% MeOH over 6 min at a flow rate of 1 mL/min; system C: 10% MeCN containing 0.1% TFA for 2 min, followed by linear gradient 10-100% over 10 min at a flow rate of 1 mL/min; and system D: 10% MeCN containing 0.1% TFA for 4 min, followed by linear gradient 10-100% over 10 min at a flow rate of 1 mL/min. Flash chromatography was performed using either glass column packed with silica gel (200−400 mesh, Aldrich Chemical) or pre-packed silica gel cartridges (FlashMaster systems, Biotage). Melting points (m.p.) were determined with an Electrothermal melting point apparatus.

Detailed procedures for the synthesis of all intermediates are included in the Supplementary Information.

*General procedures for preparations of compounds **30c-30ad**.*

A mixture of the appropriate enaminones and 1-phenylguanidine (2 equivalent mmol) in 2-methoxyethanol (3 mL) was heated at 100-140 °C for 20-45 minutes in a Discovery Microwave. Upon cooling, the residue was purified by flash chromatography using appropriate mixtures of EtOAc/PE or EtOAc/MeOH as the eluant.

 *4.1.1. 5-(5-Chloro-2-((3-(4-methylpiperazin-1-yl)phenyl)amino)pyrimidin-4-yl)-N,4-dimethyl thiazol-2-amine (**30c**)*

From 2-chloro-3-(dimethylamino)-1-(4-methyl-2-(methylamino)thiazol-5-yl)prop-2-en-1-one and 1-(3-(4-methylpiperazin-1-yl)phenyl)guanidine. Yellow solid (7%), mp 120-122 °C. Anal. RP-HPLC: t_R 13.17 min (method A), 10.82 min (method D), purity 96 %. ^{1}H-NMR (400 MHz, DMSO-d_6): δ 2.25 (3H, s), 2.34 (3H, s), 2.45-2.49 (4H, m), 2.86 (3H, d, J = 4.8 Hz), 3.13 (4H, apparent t, J = 4.8 Hz), 6.57 (1H, dd, J = 8.0 & 1.6 Hz), 7.11 (1H, apparent t, J = 8.0 Hz), 7.99 (1H, d, J = 8.0 Hz), 7.36 (1H, t, J = 2.0 Hz), 7.98 (1H, q, J = 4.8 Hz), 8.47 (1H, s), 9.52 (1H, s). ^{13}C-NMR (100 MHz, DMSO-d_6): δ 19.3, 31.3, 46.0, 48.6, 54.9, 107.0, 110.0, 110.8, 112.6, 116.3, 129.3, 141.2, 151.8, 153.6, 156.7, 158.1, 158.5, 170.2. HR-MS (ESI+): m/z [M + H]$^+$ calcd for $C_{20}H_{25}ClN_7S$, 430.1575; found 430.1675.

4.1.2. 5-(5-Chloro-2-(3-morpholinophenylamino)pyrimidin-4-yl)-N,4-dimethylthiazol-2-amine (30d)

From 1-(3-morpholinophenyl)guanidine and 2-chloro-4-methyl-1-(4-methyl-2-(methylamino)thiazol-5-yl)pent-2-en-1-one. Yellow solid (37%), mp 230-232 ºC. Anal. RP-HPLC: t_R 14.27 min (method A), 11.09 min (method D), purity 99 %. ^{1}H-NMR (400 MHz, DMSO-d_6) δ: 2.33 (3H, s), 2.87 (3H, d, J = 4.8 Hz), 3.08 (4H, apparent t, J = 4.8 Hz), 3.74 (4H, apparent t, J = 4.8 Hz), 6.58 (1H, dd, J = 8.0 & 2.0 Hz), 7.13 (1H, apparent t, J = 8.0 Hz), 7.21 (1H, d, J = 8.0 Hz), 7.38 (1H, apparent t, J = 1.6 Hz), 7.97 (1H, q, J = 4.8 Hz), 8.47 (1H, s), 9.55 (1H, s). ^{13}C-NMR (100 MHz, DMSO-d_6): δ 19.3, 31.3, 49.1, 66.6, 106.7, 109.6, 111.1, 112.6, 116.3, 129.3, 141.3, 151.9, 153.5, 156.7, 158.1, 158.5, 170.7. HR-MS (ESI+): m/z [M + H]$^+$ calcd for $C_{19}H_{22}ClN_6OS$, 417.1259; found 417.1177.

4.1.3. N,4-Dimethyl-5-(5-methyl-2-(3-morpholinophenylamino)pyrimidin-4-yl)thiazol-2-amine (30e)

From 1-(3-morpholinophenyl)guanidine and 3-(dimethylamino)-2-methyl-1-(4-methyl-2-(methylamino)thiazol-5-yl)prop-2-en-1-one. Cream (32%), mp 214-216 ℃. Anal. RP-HPLC: t_R 13.19 min (method A), 10.67 min (method D, purity 99 %). ^{1}H-NMR (400 MHz, DMSO-d_6): δ 2.15 (3H, s), 2.17 (3H, s), 2.85 (3H, d, J = 4.8 Hz), 3.08 (4H, appaent t, J = 4.8 Hz), 3.74 (4H, apparent t, J = 4.8 Hz), 6.51 (1H, dd, J = 8.0 & 2.0 Hz), 7.09 (1H, apparent t, J = 8.0 Hz), 7.19 (1H, dd, J = 8.0 & 1.2 Hz), 7.40 (1H, apparent t, J = 2.0 Hz), 7.75 (1H, q, J = 4.8 Hz, NH), 8.34 (1H,s), 9.28 (1H, s). ^{13}C-NMR (100 MHz, DMSO-d_6): δ 16.4, 18.1, 31.3, 49.3, 66.6, 106.0, 108.7, 110.4, 115.3, 118.3, 129.2, 142.1, 149.4, 151.9, 158.5, 158.6, 160.4, 169.4. HRMS (ESI$^+$): m/z [M + H]$^+$ calcd for $C_{20}H_{25}N_6OS$, 397.1805; found 397.1625.

4.1.4. 1-(4-(3-(5-Methyl-4-(2-(methylamino)thiazol-5-yl)pyrimidin-2-ylamino)phenyl)piperazin-1-yl)ethanone (30f)

From 1-(4-acetylpiperazin-1-yl)phenyl)guanidine and 3-(dimethylamino)-2-methyl-1-(4-methyl-2-(methylamino)thiazol-5-yl)prop-2-en-1-one. Light yellow powder (20%), mp 149-151 ℃. Anal. RP-HPLC: t_R 13.27 min (method A), 10.65 min (method D), purity 95 %. ^{1}H-NMR (400 MHz, DMSO-d_6): δ 2.05 (3H, s), 2.16 (3H, s), 2.18 (3H, s), 2.86 (3H, d, J = 4.8 Hz), 3.07 (2H, tm, J = 4.8 Hz), 3.14 (2H, tm, J = 4.8 Hz), 3.52-3.63 (4H, m), 6.53 (1H, dd, J = 8.0 & 2.0 Hz), 7.10 (1H, apparent t, J = 8.0 Hz), 7.22 (1H, d, J = 8.0 Hz), 7.55 (1H, t, J = 1.6 Hz), 7.82 (1H, q, J = 4.8 Hz), 8.34 (1H, s), 9.30 (1H, s). ^{13}C-NMR (100 MHz, DMSO-d_6): δ 16.4, 18.0, 21.8, 31.3, 41.2, 45.9, 49.1, 49.5, 106.8, 109.5, 110.6, 115.3, 118.4, 129.3, 142.1, 149.1, 151.7, 158.45, 158.54, 160.5, 168.7, 169.4. HRMS (ESI$^+$): m/z [M + H]$^+$ calcd for $C_{22}H_{28}N_7OS$, 438.2071, found 438.2109.

4.1.5. 1-(4-(3-((2-Amino-4,5-dihydrothiazolo[4,5-h]quinazolin-8-yl)amino)phenyl)piperazin-1-yl)ethanone (30g)

From *N′*-(6-((dimethylamino)methylene)-7-oxo-4,5,6,7-tetrahydrobenzo[d]thiazol-2-yl)-*N,N*-

dimethylformimidamide and 1-(4-acetylpiperazin-1-yl)phenyl)guanidine. Brown solid (7%), mp 291-293 ℃. Anal. RP-HPLC: t_R 10.67 min (method D), purity 95 %. ^{1}H-NMR (400 MHz, DMSO-d_6): δ 2.06 (3H, s), 2.71-2.88 (4H, m), 3.09 (2H, apparent t, $J = 4.8$ Hz), 3.16 (2H, apparent t, $J = 4.8$ Hz), 3.53-3.68 (4H, m), 6.51 (1H, dd, $J = 8.0$ & 2.0 Hz), 7.08 (1H, apparent t, $J = 8.0$ Hz), 7.18 (1H, dd, $J = 8.0$ & 0.8 Hz), 7.60 (1H, t, $J = 2.0$ Hz), 7.78 (2H, s), 8.07 (1H, s), 9.14 (1H, s). ^{13}C-NMR (125 MHz, DMSO-d_6): δ 21.7, 23.5, 25.8, 41.2, 46.0, 49.1, 49.5, 106.6, 109.2, 110.5, 115.1, 115.4, 129.2, 142.3, 151.6, 153.6, 157.6, 159.4, 159.8, 168.8, 171.9. HRMS (ESI[+]): m/z [M + H][+] calcd for $C_{21}H_{24}N_7OS$, 422.1758, found 422.1685.

4.1.6.   N,4-Dimethyl-5-(5-methyl-2-((3-(piperazin-1-yl)phenyl)amino)pyrimidin-4-yl)thiazol-2-amine (30h)

A mixture of compound **30f** 1-(4-(3-((5-methyl-4-(4-methyl-2-(methylamino)thiazol-5-yl)pyrimidin-2-yl)amino)phenyl)piperazin-1-yl)ethanone in ethanol (5 mL) and 2 M HCl (4 mL) was heated under reflux for 3 hours. After completion of the reaction, the mixture was neutralized by NaOH solution, concentrated and purified by column chromatography using $CHCl_3$/MeOH as the eluant to get the final product as cream (54%). Mp 131-133 ℃. Anal. RP-HPLC: t_R 10.90 min (method A), 8.44 min (method C), 10.47 min (method D), purity 99 %. ^{1}H-NMR (400 MHz, DMSO-d_6): δ 2.16 (3H, s), 2.17 (3H, s), 2.85 (3H, d, $J = 4.8$ Hz), 2.88 (4H, apparent t, $J = 4.8$ Hz), 3.06 (4H, apparent t, $J = 4.8$ Hz), 6.49 (1H, dd, $J = 8.0$ & 1.6 Hz), 7.07 (1H, apparent t, $J = 8.0$ Hz), 7.18 (1H, d, $J = 8.0$ Hz), 7.51 (1H, apparent t, $J = 1.6$ Hz), 7.75 (1H, q, $J = 4.8$ Hz), 8.33 (1H, s), 9.25 (1H, s). ^{13}C-NMR (100 MHz, DMSO-d6): δ 16.4, 18.1, 31.3, 45.7, 49.6, 106.33, 109.0, 110.1, 115.3, 118.3, 129.2, 142.0, 149.4, 152.4, 158.5, 158.6, 160.4, 169.4. HRMS (ESI[+]): m/z [M + H][+] calcd for $C_{20}H_{26}N_7S$, 396.1965, found 396.2151.

4.1.7. N,4-Dimethyl-5-(5-methyl-2-((3-(4-methylpiperazin-1-yl)phenyl)amino)pyrimidin-4-yl)

thiazol-2-amine (30i)

From 3-(dimethylamino)-2-methyl-1-(4-methyl-2-(methylamino) thiazol-5-yl)prop-2-en-1-one and 1-(3-(4-methylpiperazin-1-yl)phenyl)guanidine. Yellow sold (20%), mp 139-141 ºC. Anal. RP-HPLC: t_R 10.52 min (method D), purity 100 %. ^{1}H-NMR (400 MHz, DMSO-d_6): δ 2.16 (3H, s), 2.18 (3H, s), 2.23 (3H, s), 2.46 (4H, apparent t, J = 4.8 Hz), 2.85 (3H, d, J = 4.8 Hz), 3.11 (4H, apparent t, J = 4.8 Hz), 6.50 (1H, dd, J = 8.0 & 2.0 Hz), 7.07 (1H, apparent t, J = 8.0 Hz), 7.19 (1H, d, J = 8.0 & 1.2 Hz), 7.49 (1H, apparent t, J = 2.0 Hz), 7.75 (1H, q, J = 4.8 Hz), 8.33 (1H, s), 9.24 (1H, s). ^{13}C-NMR (100 MHz, DMSO-d_6): δ 16.4, 18.1, 31.3, 46.2, 48.8, 55.1, 106.3, 109.0, 110.1, 115.2, 118.3, 129.2, 142.0, 149.4, 151.9, 158.6, 158.6, 160.3, 169.4. HRMS (ESI$^+$): *m/z* [M + H]$^+$ calcd for $C_{21}H_{28}N_7S$, 410.2121; found 410.0873.

4.1.8. N,4-Dimethyl-5-(5-methyl-2-((3-(4-(methylsulfonyl)piperazin-1-yl)phenyl)amino) pyrimidin-4-yl)thiazol-2-amine (30j)

From 3-(dimethylamino)-2-methyl-1-(4-methyl-2-(methylamino)thiazol-5-yl)prop-2-en-1-one and 1-(3-(4-(methylsulfonyl)piperazin-1-yl)phenyl)guanidine. Cream (12%), mp 266-268 ºC. Anal. RP-HPLC: t_R 13.57 min (method A), 11.22 min (method D), purity 100 %. ^{1}H-NMR (400 MHz, DMSO-d_6): δ 2.16 (3H, s), 2.17 (3H, s), 2.85 (3H, d, J = 4.8 Hz), 2.93 (3H, s), 3.18-3.28 (8H, m), 6.55 (1H, dd, J = 8.0 & 2.0 Hz), 7.11 (1H, apparent t, J = 8.0 Hz), 7.24 (1H, dd, J = 8.0 & 1.2 Hz), 7.56 (1H, apparent t, J = 2.0 Hz), 7.77 (1H, q, J = 4.8 Hz), 8.34 (1H, s), 9.30 (1H, s). ^{13}C-NMR (100 MHz, DMSO-d_6): δ 16.4, 18.1, 31.3, 34.3, 45.8, 48.9, 107.0, 109.6, 110.8, 115.2, 118.4, 129.3, 142.1, 149.4, 151.3, 158.5, 160.4, 169.4. HRMS (ESI$^+$): *m/z* [M + H]$^+$ calcd for $C_{21}H_{28}N_7O_2S_2$, 474.1740; found 474.1577.

4.1.9 5-(2-((3-(1,4-Diazepan-1-yl)phenyl)amino)-5-methylpyrimidin-4-yl)-N,4-dimethylthiazol-2-amine (30k)

From 1-(4-(3-((4-(4-methyl-2-(methylamino)thiazol-5-yl)pyrimidin-2-yl)amino)phenyl)-1,4-diazepan-1-yl)ethanone, which was synthesized from 3-(dimethylamino)-2-methyl-1-(4-methyl-2-(methylamino)thiazol-5-yl)prop-2-en-1-one and 1-(3-(4-acetyl-1,4-diazepan-1-yl)phenyl)guanidine. The crude product was used in next step without further purification. Method as described for **30h**. Cream (65%), mp 121-123 ℃. Anal. RP-HPLC: t_R 10.87 min (method A), purity 99 %. ^{1}H-NMR (400 MHz, MeOH-d_4): δ 2.01-2.10 (m, 2H), 2.22 (3H, s), 2.23 (3H, s), 2.86 (apparent t, 2H, J = 5.6 Hz), 2.97 (s, 3H), 3.04 (apparent t, 2H, J = 5.2 Hz), 3.59-3.66 (4H, m), 6.41 (dd, 1H, J = 8.0 & 2.0 Hz), 6.85 (dd, 1H, J = 8.0 & 2.0 Hz), 7.10 (apparent t, 1H, J = 8.0 Hz), 7.40 (apparent t, 1H, J = 2.4 Hz), 8.28 (s, 1H). ^{13}C-NMR (100 MHz, DMSO-d_6): δ 16.4, 18.0, 29.0, 31.3, 47.5, 47.8, 48.2, 51.8, 102.3, 105.2, 106.7, 115.2, 118.2, 129.4, 142.3, 149.0, 149.2, 158.6, 158.7, 160.3, 169.3. HRMS (ESI$^+$): m/z [M + H]$^+$ calcd for $C_{21}H_{28}N_7S$, 410.2121, found 410.2049.

4.1.10. 1-(3-((5-Methyl-4-(4-methyl-2-(methylamino)thiazol-5-yl)pyrimidin-2-yl)amino)phenyl)-1,4-diazepan-5-one (30l)

From 3-(dimethylamino)-2-methyl-1-(4-methyl-2-(methylamino)thiazol-5-yl)prop-2-en-1-one and 1-(3-(5-oxo-1,4-diazepan-1-yl)phenyl)guanidine. Pale yellow solid (8 mg; 3%). Melting point: 208-209 °C. Anal. RP-HPLC: t_R 10.87 min (method B), purity 99 %. R$_f$ (9:1 CHCl$_3$:MeOH): 0.39. ν_{max} (KBr disk, cm^{-1}): 687.8, 752.0, 786.0, 847.5, 997.2, 1072.4, 1122.2, 1170.4, 1212.6, 1251.1, 1313.1, 1389.0, 1408.3, 1452.2, 1490.2, 1521.9, 1566.8, 1652.6, 2918.7, 3206.4, 3297.1. ^{1}H-NMR (400 MHz, DMSO-d_6): δ 2.15 (3H, s), 2.17 (3H, s), 2.84 (3H, d, J = 4.6 Hz), 3.12-3.23 (2H, m), 3.40-3.47 (2H, m), 3.47-3.53 (2H, m), 6.44 (1H, dd, J = 8.2 & 2.0 Hz), 7.06 (1H, apparent t, J = 8.2 Hz), 7.12-7.20 (1H, m), 7.39 (1H, m), 7.59 (1H, apparent t, J = 5.3 Hz), 7.74 (1H, q, J = 4.7 Hz), 8.32 (1H, s), 9.21 (1H, br s).* δ_H (400 MHz; CDCl$_3$): 2.22 (3H, s), 2.54 (3H, s), 2.73-2.80

(2H, m), 3.01 (3H, br s), 3.34-3.44 (2H, m), 3.55-3.60 (2H, m), 3.60-3.67 (2H, m), 5.45 (1H, br s), 5.98 (1H, br s), 6.50 (1H, dd, J = 8.2 & 2.0 Hz), 6.87 (1H, dd, J = 8.0 & 1.4 Hz), 7.05 (1H, s), 7.19 (1H, t, J = 8.2 Hz), 7.54 (1H, t, J = 2.1 Hz), 8.27 (1H, s). ^{13}C-NMR (100 MHz, DMSO-d_6): δ 15.6, 17.5, 30.7, 36.8, 40.4, 45.3, 52.3, 105.2, 108.0, 108.5, 114.6, 117.8, 129.0, 141.7, 148.8, 149.0, 157.99, 158.01, 159.8, 168.8, 175.5. HRMS (ESI$^+$): m/z [M + H]$^+$ calcd for $C_{21}H_{26}N_7OS$ 424.1914, found 424.1963. HPLC R_T (Method B, ACN): 10.80 (96%). *A CH$_2$ signal is present under the water peak, as determined by 2D experiments (COSY, HSQC).

*4.1.11.   5-(2-((3-(1,4-Diazabicyclo[3.2.2]nonan-4-yl)phenyl)amino)-5-methylpyrimidin-4-yl)-N,4-dimethylthiazol-2-amine (30m)*A suspension of 3-(1,4-diazabicyclo[3.2.2]nonan-4-yl)aniline (2.5 g; 11.5 mmol) in 20 mL acetonitrile had cyanamide (800 mg; 19.0 mmol) and TMSCl (2.9 mL; 23.0 mmol) added in sequence and the resultant suspension was heated to reflux for 18 hours, whereupon MS showed complete reaction. The ACN was decanted leaving a crude brown guanidine which was dried under vacuum (3.5 g; 92% yield as di-hydrochloride salt). 2.4 g of this material was re-dissolved in 20 mL 2-methoxyethanol and the pH adjusted with excess K_2CO_3 to pH 9 (Suspension A). A solution of *tert*-butyl *N*-methyl-*N*-(4-methyl-5-propanoyl-1,3-thiazol-2-yl)carbamate (4.0 g; 14.1 mmol) and DMF-DMA (2.4 mL; 17.5 mmol) in 12 mL ACN was heated under microwave conditions to 140 °C for 45 minutes, whereupon MS indicated near complete reaction. The reaction mixture was concentrated to dryness, azeotrophed with toluene and isopropanol, then re-dissolved in 20 mL 2-methoxyethanol. This solution was added to Suspension A and conventionally heated to reflux overnight. The reaction mixture was absorbed onto silica and purified by column chromatography, using first 9:1 CHCl$_3$:MeOH → 6:4 CHCl$_3$:MeOH (to give 1.5 g of ~ 90% pure product), which was further columned in 4:1 → 6:4 DCM:MeOH. After concentrating to dryness residue was suspended in 200 mL refluxing ether and filtered to give the

final product as a light orange solid (243 mg). A further 335 mg of product was isolated by addition of PE to the filtrate (17% yield based on starting aniline). Decomposes at 220 °C. Anal. RP-HPLC: t_R 10.92 min (method B), 10.73 min (method D), purity 97 %. ^{1}H-NMR (400 MHz, MeOH-d_4): δ 1.54-1.73 (2H, m), 1.93-2.07 (2H, m), 2.14 (3H, s), 2.15 (3H, s), 2.84 (3H, d, J = 4.7 Hz), 2.85-3.00 (6H, m), 3.42-3.51 (2H, m), 3.88 (1H, br s), 6.34 (1H, apparent dt, J = 7.3 & 2.0 Hz), 7.34 (1H, br s), 7.72 (1H, q, J = 7.5 Hz), 8.31 (1H, s), 9.15 (1H, s). ^{13}C-NMR (100 MHz, MeOH-d_4): δ 16.3, 17.2, 31.6, 43.3, 47.5, 52.5, 57.4, 106.6, 109.2, 110.3, 116.5, 120.2, 130.3, 142.8, 149.6, 151.0, 159.9, 160.0, 161.0, 172.1. HRMS (ESI$^+$): m/z [M + H]$^+$ calcd for $C_{23}H_{30}N_7S$ 436.2278, found 436.2242.

4.1.12.   1-(4-(3-((4-(4-Methyl-2-(methylamino)thiazol-5-yl)-5-(trifluoromethyl)pyrimidin-2-yl)amino)phenyl)piperazin-1-yl)ethanone (30n)

From *tert*-butyl (5-(3 (dimethylamino)-2-(trifluoromethyl)acryloyl)-4-methylthiazol-2-yl)(methyl)carbamate and 1-(3-acetylpiperazin-1-yl)phenyl)guanidine. Pale yellow solid (35%), mp 211-213 ºC. Anal. RP-HPLC: t_R 14.50 min (method A), 11.37 min (method D), purity 99 %. ^{1}H-NMR (400 MHz, DMSO-d_6): δ 2.05 (3H, s), 2.16 (3H, s), 2.85 (3H, d, J = 4.8 Hz), 3.08 (2H, apparent t, J = 4.8 Hz), 3.14 (2H, apparent t, J = 4.8 Hz), 3.54-3.64 (4H, m), 6.66 (1H, d, J = 8.0 Hz), 7.17 (1H, apparent t, J = 8.0 Hz), 7.22 (1H, d, J = 8.0 Hz), 7.45 (1H, s), 7.85 (1H, q, J = 4.8 Hz), 8.78 (1H, s), 10.11 (1H, s). ^{13}C-NMR (100 MHz, DMSO-d$_6$): δ 17.4, 21.7, 31.3, 41.1, 45.9, 48.9, 49.3, 108.2, 111.2, 111.9, 112.5 (q, J = 25 Hz), 124.8 (q, J = 216 Hz), 129.5, 140.4, 150.6, 151.6, 158.1, 158.7, 160.9, 168.7, 169.7. HRMS (ESI$^+$): m/z [M + H]$^+$ calcd for $C_{22}H_{25}F_3N_7OS$, 492.1788; found 492.1743.

4.1.13.   N,4-Dimethyl-5-(2-((3-(piperazin-1-yl)phenyl)amino)-5-(trifluoromethyl)pyrimidin-4-yl)thiazol-2-amine (30o)

From compound **30n** 1-(4-(3-((4-(4-methyl-2-(methylamino)thiazol-5-yl)-5-(trifluoromethyl)

pyrimidin-2-yl)amino)phenyl)piperazin-1-yl)ethanone. Method as described from **30f**. Yellow

solid (68%), mp 207-209 ℃. Anal. RP-HPLC: t_R min (method A), 10.80 min (method D), purity

99 %. ^{1}H-NMR (400 MHz, DMSO-d_6): δ 2.15 (3H,s), 2.85 (3H, d, J = 4.8 Hz), 2.95 (4H, apparent

t, J = 4.8 Hz), 3.12 (4H, apparent t, J = 4.8 Hz), 6.66 (1H, d, J = 8.0 Hz), 7.15 (1H, apparent t, J =

8.0 Hz), 7.20 (1H, d, J = 8.0 Hz), 7.42 (1H, s), 7.86 (1H, q, J = 4.8 Hz), 8.77 (1H, s), 10.09 (1H,

s). ^{13}C-NMR (100 MHz, DMSO-d_6): δ 14.55, 32.28, 44.98, 48.56, 107.95, 110.97, 111.71, 112.48

(q, J = 25 Hz), 124.76 (q, J = 216 Hz), 129.44, 140.40, 150.90, 151.94, 158.02, 158.83, 160.87,

169.74. HRMS (ESI$^+$): m/z [M + H]$^+$ calcd for $C_{20}H_{23}F_3N_7S$, 450.1688; found 450.1332.

4.1.14. N,4-Dimethyl-5-(2-((3-morpholinophenyl)amino)-5-vinylpyrimidin-4-yl)thiazol-2-amine

(30p)

From 5-(5-chloro-2-((3-morpholinophenyl)amino)pyrimidin-4-yl)-N,4-dimethylthiazol-2-amine.

Yellow solid (60%). ^{1}H-NMR (500 MHz; DMSO-d_6): δ 2.09 (3H, s), 2.86 (3H, d, J = 4.8 Hz),

3.11 (4H, apparent t, J = 4.8 Hz), 3.75 (4H, apparent t, J = 4.8 Hz), 5.23 (1H, d, J = 12.0 Hz), 6.51

(1H, d, J = 17.6 Hz), 6.45-6.60 (2H, m), 7.11 (1H, apparent t, J = 8.0 Hz), 7.19 (1H, d, J = 8.0 Hz),

7.60 (1H, s), 7.84 (1H, q, J = 4.8 Hz), 8.76 (1H,s), 9.57 (1H, s). ^{13}C-NMR (125 MHz, DMSO-d_6):

δ 18.4, 31.3, 49.3, 66.6, 106.2, 109.2, 110.7, 113.6, 115.3, 119.6, 129.3, 132.2, 141.6, 150.2, 152.0,

157.2, 157.3, 158.8, 169.9. HRMS (ESI$^+$): m/z [M + H]$^+$ calcd for $C_{21}H_{25}N_6OS$, 409.1805, found

409.1680.

4.1.15.1-(4-(3-((5-Bromo-4-(4-methyl-2-(methylamino)thiazol-5-yl)pyrimidin-2-

yl)amino)phenyl)piperazin-1-yl)ethanone (30q)

From *tert*-butyl (5-(5-bromo-2-chloropyrimidin-4-yl)-4-methylthiazol-2-yl)(methyl)carbamate

and 1-(4-(3-aminophenyl)piperazin-1-yl)ethanone. Yellow solid (28%), mp 205-207 ℃. Anal. RP-

HPLC: t_R 10.52 min (method D), purity 100 %. ^{1}H-NMR (400 MHz, DMSO-d_6): δ 2.05 (3H, s), 2.30 (3H, s), 2.87 (3H, d, J = 4.8 Hz), 3.08 (2H, apparent t, J = 4.8 Hz), 3.14 (2H, apparent t, J = 4.8 Hz), 3.50-3.53 (4H, m), 6.59 (1H, dd, J = 8.0 & 1.6 Hz), 7.13 (1H, apparent t, J = 8.0 Hz), 7.20 (1H, br d, J = 8.0 Hz), 7.42 (1H, br s), 7.41 (1H, q, J = 4.8 Hz), 8.57 (1H, s), 9.60 (1H, s). ^{13}C-NMR (100 MHz, DMSO-d_6): δ 19.1, 21.7, 31.3, 41.1, 45.9, 49.4, 106.3, 107.5, 110.3, 111.2, 114.0, 129.4, 141.2, 151.7, 152.4, 158.2, 158.5, 161.0, 168.7, 169.8. HRMS (ESI$^+$): m/z [M + H]$^+$ calcd for $C_{21}H_{25}BrN_7OS$, 502.1019, found 502.1035.

*4.1.16. 5-(2-((3-(1,4-Diazepan-1-yl)phenyl)amino)pyrimidin-4-yl)-N-methyl-4-(trifluoromethyl)thiazol-2-amine (**30r**)*

From 1-(4-(3-((4-(2-(methylamino)-4-(trifluoromethyl)thiazol-5-yl)pyrimidin-2-yl)amino) phenyl)-1,4-diazepan-1-yl)ethanone. Method as described from **45**. Yellow solid (64%), mp 194-196 ºC. Anal. RP-HPLC: t_R 12.10 min (method B), 11.75 (method D), purity 100%. ^{1}H-NMR (400 MHz, DMSO-d_6): δ 1.85-1.72 (2H, m), 2.62 (2H, apparent t, J = 5.6 Hz), 2.84 (2H, apparent t, J = 5.2 Hz), 2.89 (3H, s), 3.46 (2H, apparent t, J = 5.2 Hz), 3.54 (2H, apparent t, J = 6.0 Hz), 6.29-6.41 (1H, m), 6.92 (1H, d, J = 5.2 Hz), 7.10-6.98 (3H, m), 8.46 (1H, br s), 8.48 (1H, d, J = 5.2 Hz), 9.42 (1H, s). ^{13}C-NMR (100 MHz, DMSO-d_6): δ 29.5, 31.4, 47.8, 47.9, 48.5, 49.1, 52.7, 102.7, 106.0, 107.0, 108.7, 121.3 (q, J = 270 Hz), 126.0, 129.5, 137.3 (q, J = 34 Hz), 141.5, 149.1, 156.0, 159.4, 160.2, 170.0. HRMS (ESI$^+$): m/z [M + H]$^+$ calcd for $C_{20}H_{23}F_3N_7S$, 450.1682, found 450.1458.   1-(4-(3-((4-(2-(Methylamino)-4-(trifluoromethyl)thiazol-5-yl)pyrimidin-2-yl)amino)phenyl)-1,4-diazepan-1-yl)ethanone. From *tert*-butyl methyl(5-(4-methylpent-2-enoyl)-4-(trifluoromethyl)thiazol-2-yl)carbamate and 1-(3-(4-acetyl-1,4-diazepan-1-yl)phenyl)guanidine. Yellow solid (53%). ^{1}H-NMR (400 MHz, DMSO-d_6): δ 1.92-1.77 (3.5H, m), 1.99 (1.5H, s), 2.89 (3H, d, J = 3.6 Hz), 3.38-3.27 (2H, m), 3.60-3.46 (6H, m), 6.43-6.36 (1H, m), 6.92 (1H, d, J = 4.8

Hz), 7.18-7.02 (3H, m), 8.46 (1H, br s), 8.49 (d, 1H, J = 5.2 Hz), 9.45 (d, 1H, J = 3.6 Hz). HRMS (ESI$^+$): m/z [M + H]$^+$ calcd for $C_{22}H_{25}F_3N_7OS$, 492.1788, found 492.1731.

4.1.17. 5-(2-((3-(1,4-diazepan-1-yl)phenyl)amino)pyrimidin-4-yl)-N-methylthiazol-2-amine (30s)

From 1-(4-(3-((4-(2-(methylamino)thiazol-5-yl)pyrimidin-2-yl)amino)phenyl)-1,4-diazepan-1-yl) ethanone (From *tert*-butyl (5-(3-(dimethylamino)acryloyl)thiazol-2-yl)(methyl)carbamate and 1-(3-(4-acetyl-1,4-diazepan-1-yl)phenyl)guanidine. After completion of the reaction, the product was purified by EtOAc/MeOH to get the crude product and used in the next reaction directly). Method as described from **45**. Grey solid (62%), mp 139-141 ºC. Anal. RP-HPLC: t_R 10.87 min (method B), 10.48 min (method D), purity 100%. ^{1}H-NMR (400 MHz, DMSO- d_6): δ 1.76-1.87 (2H, m), 2.63 (2H, apparent t, J = 5.2 Hz), 2.86 (2H, apparent t, J = 5.2 Hz), 2.89 (3H, d, J = 4.8 Hz), 3.48 (2H, apparent t, J = 5.2 Hz), 3.56 (2H, apparent t, J = 6.0 Hz), 6.26-6.35 (1H, m), 6.98-7.00-7.13 (2H, m), 7.11 (1H, d, J = 5.2 Hz), 7.22 (1H, s), 8.03 (1H, s), 8.18 (1H, q, J = 4.8 Hz), 8.27 (1H, d, J = 5.2 Hz), 9.16 (1H, s). ^{13}C-NMR (100 MHz, DMSO- d_6): δ 29.4, 31.4, 47.7, 47.9, 48.2, 52.3, 102.4, 105.5, 105.6, 106.9, 124.6, 129.5, 142.1, 143.1, 149.1, 157.6, 158.9, 160.4, 172.7. HRMS (ESI$^+$): m/z [M + H]$^+$ calcd for $C_{19}H_{24}N_7S$, 382.1808, found 382.1975.

4.1.18.   3-((4-(4-Cyclopropyl-2-(methylamino)thiazol-5-yl)pyrimidin-2-yl)amino)-N-(1-methyl piperidin-4-yl)benzamide (30t)

From *tert*-butyl (4-cyclopropyl-5-(3-(dimethylamino)acryloyl)thiazol-2-yl)(methyl)carbamate and 3-guanidino-*N*-(1-methylpiperidin-4-yl)benzamide. Cream (24%), mp 254-256 °C. Anal. RP-HPLC: t_R min 11.30 (method A), 8.57 (method C), 10.65 (method D), purity 98 %. ^{1}H-NMR (400 MHz, DMSO- d_6): δ 0.90-1.05 (4H, m), 1.50-1.65 (2H, m), 1.72-1.82 (2H, m), 1.94 (2H, t, J = 11.6 Hz), 2.17 (3H, s), 2.58-2.68 (1H, m), 2.76 (2H, d, J = 11.6 Hz), 2.82 (3H, d, J = 4.8 Hz), 3.66-3.78 (1H, m), 7.01 (1H, d, J = 5.6 Hz), 7.39-7.41 (2H, m), 7.91 (1H, d, J = 8.0 Hz), 8.03 (1H,

q, J = 4.8 Hz), 8.09-8.18 (2H, m), 8.33 (1H, d, J = 5.6 Hz), 9.52 (1H, s). ¹³C-NMR (100 MHz,

DMSO-d_6): δ 9.2, 13.1, 31.3, 31.9, 46.5, 47.0, 55.0, 108.1, 117.3, 119.0, 120.4, 121.9, 128.5, 136.1,

141.1, 158.1, 158.3, 159.3, 159.9, 166.7, 170.0. HRMS (ESI⁺): m/z [M + H]⁺ calcd for

$C_{24}H_{30}N_7OS$, 464.2227; found 464.2436.

4.1.19. 1-(4-(3-((4-(4-Isopropyl-2-(methylamino)thiazol-5-yl)pyrimidin-2-yl)amino)phenyl)

piperazin-1-yl)ethanone (30u)

From *tert*-butyl (5-(3-(dimethylamino)acryloyl)-4-isopropylthiazol-2-yl)(methyl)carbamate and

1-(4-acetylpiperazin-1-yl)phenyl)guanidine. Yellow solid (15%), mp 190-192 ℃. Anal. RP-

HPLC: t_R 11.19 min (method D), purity 100 %. ¹H-NMR (400 MHz, DMSO-d_6): δ 1.24 (6H, d, J

= 5.2 Hz), 2.05 (3H, s), 2.85 (3H, d, J = 4.8 Hz), 3.11 (2H, apparent t, J = 4.8 Hz), 3.17 (2H,

apparent t, J = 4.8 Hz), 3.48-3.51 (1H, m), 3.51-3.53 (4H, m), 6.58 (1H, dd, J = 8.0 & 2.0 Hz),

6.83 (1H, d, J = 5.6 Hz), 7.12 (1H, apparent t, J = 8.0 Hz), 7.22 (1H, dd, J = 8.0 & 0.8 Hz), 7.44

(1H, t, J = 2.0 Hz), 8.07 (1H, q, J = 4.8 Hz), 8.33 (1H, d, J = 5.6 Hz), 9.28 (1H, s). ¹³C-NMR (100

MHz, DMSO-d_6): δ 21.7, 22.5, 29.6, 31.5, 41.2, 45.98, 49.1, 49.6, 107.2, 107.8, 110.0, 111.1,

117.3, 129.3, 141.8, 151.7, 158.4, 158.9, 160.1, 162.2, 168.7, 170.5. HRMS (ESI⁺): m/z [M + H]⁺

calcd for $C_{23}H_{30}N_7OS$, 452.2227; found 452.2418.

4.1.20. 1-(4-(3-(4-(4-Methyl-2-(methylamino)thiazol-5-yl)pyrimidin-2-ylamino)phenyl)

piperazin-1-yl)ethanone (30v)

From 1-(4-acetylpiperazin-1-yl)phenyl)guanidine and 3-(dimethylamino)-1-(4-methyl-2-(methyl

amino)thiazol-5-yl)prop-2-en-1-one. Light yellow powder (78%), mp 217-219 ℃. Anal. RP-

HPLC: t_R 13.42 min (method A), 10.62 min (method D), purity 100 %. ¹H-NMR (400 MHz,

DMSO-d_6): δ 2.05 (3H, s), 2.47 (3H, s), 2.86 (3H, d, J = 4.8 Hz), 3.11 (2H, apparent t, J = 5.2 Hz),

3.17 (2H, apparent t, J = 5.2 Hz), 3.54-3.64 (4H, m), 6.57 (1H, dd, J = 8.0 & 1.6 Hz), 6.90 (1H, d,

J = 5.6 Hz), 7.12 (1H, apparent t, *J* = 8.0 Hz), 7.22 (1H, d, *J* = 8.0 Hz), 7.55 (1H, apparent t, *J* = 1.6 Hz), 8.05 (1H, q, *J* = 4.8 Hz), 8.33 (1H, d, *J* = 5.6 Hz), 9.28 (1H, s). ^{13}C-NMR (100 MHz, DMSO-*d₆*): δ 19.1, 21.7, 31.3, 41.2, 46.0, 49.1, 49.6, 107.1, 107.1, 109.9, 111.0, 118.4, 129.3, 141.8, 151.7, 152.7, 158.1, 159.1, 160.1, 168.7, 169.8. HRMS (ESI$^+$): *m/z* [M + H]$^+$ calcd for C$_{21}$H$_{26}$N$_7$OS, 424.1914; found 424.1955.

*4.1.21. 2-((3-(Azepan-1-yl)phenyl)amino)-4-(4-methyl-2-(methylamino)thiazol-5-yl)pyrimidine-5-carbonitrile (**30w**)*

From 3-(dimethylamino)-2-(4-methyl-2-(methylamino)thiazole-5-carbonyl)acrylonitrile and 1-(3-(azepan-1-yl)phenyl)guanidine. Pale yellow solid (32%). Melting point: 249-252 °C. Anal. RP-HPLC: t_R 13.15 min (method B), 11.75 min (method D), purity 99 %. ^{1}H-NMR (400 MHz, DMSO-*d₆*): δ 1.45 (4H, br s), 1.72 (4H, br s), 2.38 (3H, s), 2.87 (3H, s), 3.44 (4H, br t, *J* = 6.0 Hz), 6.39 (1H, dd, *J* = 8.0 & 1.6 Hz), 6.97-7.10 (3H, m), 8.21 (1H, br s), 8.74 (1H, s), 9.84 (1H, br s). ^{13}C-NMR (100 MHz, DMSO-*d₆*): δ 19.3, 26.3, 26.8, 30.7, 48.7, 93.7, 103.3, 106.4, 107.6, 117.7, 129.0, 139.7, 148.6, 158.9, 161.0, 163.2, 170.0. HRMS (ESI$^+$): *m/z* [M + H]$^+$ calcd for C$_{22}$H$_{26}$N$_7$S 420.1965, found 420.1969.

*4.1.22.   2-((3-(Azepan-1-yl)-5-methylphenyl)amino)-4-(4-methyl-2-(methylamino)thiazol-5-yl) pyrimidine-5-carbonitrile (**30x**)*

From 3-(dimethylamino)-2-(4-methyl-2-(methylamino)thiazole-5-carbonyl)acrylonitrile and 1-(3-(azepan-1-yl)-5-methylphenyl)guanidine. Yellow solid (18% over three steps). Melting point: 217-219 °C. Anal. RP-HPLC: t_R 13.42 min (method B), 11.20 min (method D), purity 99 %. ^{1}H-NMR (500 MHz; DMSO-*d₆*): δ 1.35-1.52 (4H, m), 1.62-1.81 (4H, m), 2.21 (3H, s), 2.39 (3H, br s), 2.87 (3H, d, *J* = 4.8 Hz), 3.42 (4H, t, *J* = 6.0 Hz), 6.23 (1H, s), 6.85 (1H, s), 6.88 (1H, s), 8.34 (1H, q, *J* = 4.6 Hz), 8.74 (1H, s), 9.96 (1H, br s). ^{13}C-NMR (150 MHz; DMSO-*d₆*): δ 19.9, 22.4,

26.7, 27.5, 31.3, 49.3, 93.7, 101.2, 107.7, 109.1, 118.4, 138.5, 140.1, 149.1, 155.0, 159.5, 161.5, 163.7, 170.6. HRMS (ESI⁺): m/z [M + H]⁺ calcd for $C_{23}H_{28}N_7S$ 434.2121, found 436.2106.

4.1.23.   4-(4-Methyl-2-(methylamino)thiazol-5-yl)-2-((3-methyl-5-(piperazin-1-yl)phenyl)

amino)pyrimidine-5-carbonitrile (30y)

From 3-(dimethylamino)-2-(4-methyl-2-(methylamino)thiazole-5-carbonyl)acrylonitrile and 1-(3-methyl-5-(piperazin-1-yl)phenyl)guanidine. Brown solid (76%). Melting point: 119-121 °C. Anal. RP-HPLC: t_R 11.42 min (method B), 10.97 min (method D), purity 95 %. ¹H-NMR (400 MHz; DMSO-d_6): δ 2.23 (3H, s), 2.40 (3H, br s), 2.78-2.85 (4H, m), 2.88 (3H, d, J = 4.7 Hz), 2.98-3.06 (4H, m), 6.47 (1H, s), 7.02 (1H, s), 7.13 (1H, br s), 8.24 (1H, q, J = 4.7 Hz), 8.75 (1H, s), 10.00 (1H, br s). ¹³C-NMR (150 MHz; DMSO-d_6): δ 19.5, 21.7, 30.9, 45.6, 49.6, 93.3, 105.1, 111.5, 112.1, 117.9, 137.9, 139.3, 152.0, 154.9, 159.0, 161.0, 163.4, 170.2. HRMS (ESI⁺): m/z [M + H]⁺ calcd for $C_{21}H_{25}N_8S$ 421.1917, found 421.1921.

4.1.24.   4-(4-Methyl-2-(methylamino)thiazol-5-yl)-2-((3-methyl-5-morpholinophenyl)amino)

pyrimidine-5-carbonitrile (30z)

From 3-(dimethylamino)-2-(4-methyl-2-(methylamino)thiazole-5-carbonyl)acrylonitrile and 1-(3-methyl-5-morpholinophenyl)guanidine. Yellow solid (55%). Melting point: 243-245 °C. Anal. RP-HPLC: t_R 12.67 min (method B), 11.52 min (method D), purity 96 %. ¹H-NMR (400 MHz; DMSO-d_6): δ 2.24 (3H, s), 2.39 (3H, br s), 2.87 (3H, s), 3.05-3.12 (4H, m), 3.68-3.82 (4H, m), 6.50 (1H, s), 7.05 (1H, s), 7.15 (1H, s), 8.24 (1H, br s), 8.75 (1H, s), 10.03 (1H, br s). ¹³C-NMR (100 MHz; DMSO-d_6): δ 19.5, 21.6, 30.8, 48.7, 66.1, 93.3, 104.8, 111.2, 112.6, 117.8, 138.1, 139.4, 151.4, 156.0, 161.0, 163.4, 170.2. HRMS (ESI⁺): m/z [M + H]⁺ Calculated for $C_{23}H_{28}N_7S$ 422.1758, found 422.1770.

4.1.25.   5-(2-((3,5-Dimorpholinophenyl)amino)pyrimidin-4-yl)-N,4-dimethylthiazol-2-amine (30aa)

From 3-(dimethylamino)-1-(4-methyl-2-(methylamino)thiazol-5-yl)prop-2-en-1-one and 1-(3,5-dimorpholinophenyl)guanidine. Pale yellow solid (2%). Decomposes at 205 °C. Anal. RP-HPLC: t_R 11.30 min (method B), 10.63 min (method D), purity 97 %. ^{1}H-NMR (400 MHz; DMSO-d_6): δ 2.44 (3H, s), 2.84 (3H, d, J = 4.8 Hz), 3.00-3.20 (8H, m), 3.64-3.81 (8H, m), 6.13 (1H, s), 6.88 (1H, d, J = 5.5 Hz), 6.94 (1H, d, J = 1.9 Hz), 8.04 (1H, q, J = 4.6 Hz), 8.31 (1H, d, J = 5.4 Hz), 9.10 (1H, s). ^{13}C-NMR (150 MHz; DMSO-d_6): δ 18.7, 30.7, 49.2, 66.2, 97.2, 98.4, 106.6, 117.9, 141.7, 152.2, 152.3, 157.6, 158.5, 159.7, 169.5. HRMS (ESI[+]): m/z [M + H][+] calcd for $C_{23}H_{30}N_7O_2S$ 468.2176, found 468.2203.

4.1.26.   1,1'-(4,4'-(5-((4-(4-Methyl-2-(methylamino)thiazol-5-yl)pyrimidin-2-yl)amino)-1,3-phenylene)bis(piperazine-4,1-diyl))diethanone (30ab)

From 3-(dimethylamino)-1-(4-methyl-2-(methylamino)thiazol-5-yl)prop-2-en-1-one and 1-(3,5-bis(4-acetylpiperazin-1-yl)phenyl)guanidine. Pale yellow solid (16%). Melting point: 200-202 °C. Anal. RP-HPLC: t_R 12.94 min (method B), 10.32 min (method D), purity 95 %. ^{1}H-NMR (400 MHz; DMSO-d_6; 1:1 mix of rotamers): δ 2.04 (6H, s), 2.46 (3H, s), 2.85 (3H, d, J = 4.8 Hz), 3.05-3.11 (4H, m), 3.12-3.18 (4H, m), 3.51-3.61 (8H, m), 6.17 (1H, s), 6.89 (1H, d, J = 5.6 Hz), 6.96 (2H, d, J = 1.9 Hz), 8.05 (1H, d, J = 4.8 Hz), 8.31 (1H, d, J = 5.4 Hz), 9.13 (1H, s). ^{13}C-NMR (125 MHz; DMSO-d_6; mix of rotamers): δ 18.7, 21.7, 31.0, 40.8, 45.6, 49.0, 49.4, 98.9, 99.3, 106.5, 117.9, 141.7, 151.9, 152.3, 157.6, 158.5, 159.6, 168.3, 169.5. HRMS (ESI[+]): m/z [M + H][+] calcd for $C_{27}H_{36}N_9O_2S$ 550.2707, found 550.2749.

4.1.27.2-((3,5-Dimorpholinophenyl)amino)-4-(4-methyl-2-(methylamino)thiazol-5-yl)pyrimidine-5-carbonitrile (30ac)

From 3-(dimethylamino)-2-(4-methyl-2-(methylamino)thiazole-5-carbonyl)acrylonitrile and 1-(3,5-dimorpholinophenyl)guanidine. Pale yellow solid (2%). Melting point: 180-182 °C. Anal. RP-HPLC: t_R 11.95 min (method B), 10.94 min (method D), purity 100 %. ^{1}H-NMR (400 MHz; DMSO-d_6): δ 2.36 (3H, br s), 2.88 (3H, d, J = 4.1 Hz), 3.07 (8H, dd, J = 6.9 & 4.7 Hz), 3.73 (8H, dd, J = 6.3 & 4.8 Hz), 6.23 (1H, s), 6.91 (2H, s), 8.34 (1H, br s), 8.76 (1H, s), 10.00 (1H, br s). ^{13}C-NMR (100 MHz; DMSO-d_6): δ 19.3, 31.0, 49.0, 66.1, 93.6, 98.7, 99.2, 100.0, 117.8, 140.0, 152.0, 159.0, 163.5. HRMS (ESI$^+$): m/z [M + H]$^+$ calcd for $C_{24}H_{29}N_8O_2S$ 493.2129, found 493.2134.

4.1.28. 2-((3,5-Bis(4-acetylpiperazin-1-yl)phenyl)amino)-4-(4-methyl-2-(methylamino)thiazol-5-yl)pyrimidine-5-carbonitrile (30ad)

From 3-(dimethylamino)-2-(4-methyl-2-(methylamino)thiazole-5-carbonyl)acrylonitrile and 1-(3,5-bis(4-acetylpiperazin-1-yl)phenyl)guanidine. Decomposes at 167 °C. Anal. RP-HPLC: t_R 13.47 min (method B), 10.72 min (method D), purity 100 %. ^{1}H-NMR (400 MHz; DMSO-d_6; 1:1 mix of rotamers): δ 2.04 (6H, s), 2.36 (3H, br s), 2.87 (3H, d, J = 4.7 Hz), 3.02-3.11 (4H, m), 3.12-3.17 (4H, m), 3.46-3.66 (8H, m), 6.27 (1H, d, J = 2.1 Hz), 6.91 (2H, d, J = 2.0 Hz), 8.33 (1H, br s), 8.76 (1H, s), 10.0 (1H, br s). ^{13}C-NMR (125 MHz; DMSO-d$_6$; mix of rotamers): δ 19.5, 21.2, 30.9, 40.7, 45.5, 48.7, 49.1, 93.5, 100.0, 100.6, 140.0, 151.9, 159.0, 161.1, 136.2, 168.3, 170.2. HRMS (ESI$^+$): m/z [M + H]$^+$ calcd for $C_{28}H_{35}N_{10}O_2S$ 575.2660, found 575.2664.

4.1.29. 1,1'-(4,4'-(5-((5-Methyl-4-(4-methyl-2-(methylamino)thiazol-5-yl)pyrimidin-2-yl)amino)-1,3-phenylene)bis(piperazine-4,1-diyl))diethanone (30ae)

From 3-(dimethylamino)-2-methyl-1-(4-methyl-2-(methylamino)thiazol-5-yl)prop-2-en-1-one and 1-(3,5-bis(4-acetylpiperazin-1-yl)phenyl)guanidine. Pale yellow solid (10%). Melting point: 121-123 °C. Anal. RP-HPLC: t_R 10.34 min (method A), 10.34 min (method D), purity 95 %. ^{1}H-

NMR (400 MHz; CDCl$_3$; 1:1 mix of rotamers): δ 2.13 (6H, s), 2.22 (3H, s), 2.23 (3H, s) , 3.02 (3H, d, J = 3.8 Hz), 3.14-3.22 (8H, m), 3.55-3.65 (4H, m), 3.71-3.80 (4H, m), 5.63 (1H, br s), 6.17 (1H, apparent t, J = 2.0 Hz), 6.90 (2H, d, J = 2.0 Hz), 7.04 (1H, s), 8.27 (1H, s). ^{13}C-NMR (100 MHz; CDCl$_3$; mix of rotamers): δ 16.2, 17.7, 21.3, 32.0, 41.4, 46.3, 49.7, 50.1, 100.2, 100.5, 116.3, 119.1, 141.6, 149.2, 152.5, 158.9, 160.0, 169.0, 170.8. HRMS (ESI$^+$): m/z [M + H]$^+$ calcd for C$_{28}$H$_{38}$N$_9$O$_2$S 564.2864, found 564.2852.

4.2. Molecular Modelling

Modelling was performed using OpenEye OEDocking software. Up to 2000 conformations of the individual compounds to be docked were generated using OpenEye OMEGA program and docked using OpenEye FRED into receptors generated by the OpenEye MAKE RECEPTOR program using default settings from reported crystal structures for CDK9 ([4BCF] and [4BCG]) and CDK2 ([4BCP] and [4BCO]). FRED Chemgauss 4 was used as the scoring function. The number of alternate poses retuned was set to 20 and all other settings were on default. Results were visualised using OpenEye VIDA software and images generated using DeLano Scientific LLC PyMOL freeware.

4.3. Biological assays

4.3.1 Kinase assay

Inhibition of CDKs and other kinases was measured by radiometric assay using the Millipore KinaseProfiler services using K$_{m(app)}$ concentration of ATP of each kinase. Half-maximal inhibition (IC$_{50}$) values were calculated from 10-point dose-response curves and apparent inhibition constants (K_i) were calculated from the IC$_{50}$ values and appropriate K_m (ATP) values for the kinases in question.

4.3.2. Cell culture

Cancer cell lines were obtained from the American Type Tissue Collection (ATTC) global bioresource centre and cultured in RPMI-1640 with 10% FBS.

4.3.3. Proliferation assays

MTT (3-(4,5-dimethylthiazol-2-yl)-2,5-diphenyltetrazolium bromide, Sigma) assays were performed as reported previously.[35] Compound concentrations required to inhibit 50% of cell growth (GI_{50}) were calculated using non-linear regression analysis.

4.3.4. Caspase-3 assay

Activity of caspase 3 was measured using the fuorimetric caspase 3 assay kit (Sigma-Aldrich, cat: CASP3F-1KT). Method as described from the kit.

4.3.5. Cell cycle analysis and detection of apoptosis

Cells (4×10^5) were cultured for 24 h in medium alone or with varying concentrations of inhibitor. Cells were harvested and prepared in hypotonic fluorochrome solution (0.1% sodium citrate; 0.1% Triton X-100; 50μg/ml propidium iodide; 100ug/ml RNase A in dH_2O). Cell cycle status was analyzed using a Beckman Coulter EPICS-XL MCL^{TM} flow cytometer and data were analyzed using EXPO32^{TM} software.

Apoptotic populations were examined using FITC annexinV/PI (Annexin V-FITC Apoptosis Detection Kit I, BD Biosciences, cat: 556547) staining after cells were cultured in medium only or with varying concentrations of inhibitors according to the protocols (BD Bioscience). The annexin V/PI-positive apoptotic cells were enumerated using a Beckman Coulter EPICS-XL MCL^{TM} flow cytometer.

4.3.6. Detection of apoptosis in primary CLL cells

Freshly isolated primary CLL cells and normal B- and T-cells were cultured in RPMI with 10% foetal calf serum and L-glutamine, penicillin, and streptomycin. Cells were maintained at 37 °C in

an atmosphere containing 95% air and 5% CO_2 (vol/vol). CLL cells (10^6/mL) were treated with inhibitor for 48 h. Subsequently, cells were labelled with CD19-APC (Caltag) and then re-suspended in 200 µL binding buffer containing 4 µL annexin V–FITC (Bender Medsystems, Vienna, Austria). Apoptosis was quantified in the CD19+ CLL cells, CD19+ normal B-cells and CD3+ normal T-cells using an Accuri C6 flow cytometer and FlowJo software (TreeStar). LD_{50} values were calculated from line-of-best-fit analysis of the sigmoidal dose response curves.

4.3.7. Western blots

Western blotting was performed as described.[25] Antibodies used were as follows: total RNAP-II (8WG16), phosphorylated RNAP-II Ser-2, phosphorylated RNAP-II Ser-5 (Covance), p53 (Dako), β-actin (Sigma-Aldrich), Mcl-1, Cleaved PARP (Cell Signalling Technologies), p21 (Santa Cruz). Both anti-mouse and anti-rabbit immunoglobulin G (IgG) horse-radish peroxidase-conjugated antibodies were obtained from Dako.

4.3.8. Statistical analysis

All experiments were performed in triplicate and repeated at least twice; representative experiments were selected for figures. Statistical significance was determined using one-way analysis of variance (ANOVA), with a minimal level of significance at $p < 0.01$.

Author Contributions

[1] These authors contributed equally. The manuscript was written through contributions of all authors. All authors have given approval to the final version of the manuscript.

Declaration of competing interest

The authors declare that they have no known competing financial interests or personal relationships that could have appeared to influence the work reported in this paper.

Appendix A. Supplementary data

Detailed procedures for the synthesis of all intermediates and the biological mechanism of actions of compound **30k** can be found online at

ABBREVIATIONS

ALL; acute lymphocytic leukaemia; ATP, adenosine triphosphate; Bcl-2, B-cell lymphoma 2; CDK, cyclin-dependent kinase; CTD, carboxyl terminal domain; DCM, dichloromethane; DMF, *N,N*-dimethylformamide; DMF-DMA, dimethylformamide dimethyl acetal; DMSO, dimethylsulfoxide; DMAP: dimethylaminopyridine; HRMS, high resolution mass spectra; KDR, Kinase Insert Domain Receptor; LDA, Lithium diisopropylamide; Mcl-1, myeloid cell leukaemia sequence 1; MeCN, Acetonitrile; MLK1, Mixed-Lineage Kinase 1; NBS, *N*-bromosuccinimide; NCS, *N*-chlorosuccinimide; NELF, negative elongation factor; NEK2 , NIMA Related Kinase 2; PARP, poly(ADP-ribose) polymerase; P-TEFb, positive transcription elongation factor b; SAR, structure and activity relationships.

Reference

[1] M. Malumbres, M. Barbacid, Mammalian cyclin-dependent kinases, Trends Biochem. Sci., 30 (2005) 630-641.

[2] J. Chou, D.A. Quigley, T.M. Robinson, F.Y. Feng, A. Ashworth, Transcription-Associated Cyclin-Dependent Kinases as Targets and Biomarkers for Cancer Therapy, Cancer Discov., 10 (2020) 351-370.

[3] P.K. Parua, R.P. Fisher, Dissecting the Pol II transcription cycle and derailing cancer with CDK inhibitors, Nat. Chem. Biol., 16 (2020) 716-724.

[4] S. Wang, P.M. Fischer, Cyclin-dependent kinase 9: a key transcriptional regulator and potential drug target in oncology, virology and cardiology, Trends Pharmacol. Sci., 29 (2008) 302-313.

[5] G. Romano, A. Giordano, Role of the cyclin-dependent kinase 9-related pathway in mammalian gene expression and human diseases, Cell Cycle, 7 (2008) 3664-3668.

[6] B. Palancade, O. Bensaude, Investigating RNA polymerase II carboxyl-terminal domain (CTD) phosphorylation, Europ. J. Biochem., 270 (2003) 3859-3870.

[7] J. Garriga, X. Grana, Cellular control of gene expression by T-type cyclin/CDK9 complexes, Gene, 337 (2004) 15-23.

[8] C.W. Bacon, I. D'Orso, CDK9: a signaling hub for transcriptional control, Transcription, 10 (2019) 57-75.

[9] A.M. Mandelin, 2nd, R.M. Pope, Myeloid cell leukemia-1 as a therapeutic target, Expert Opin. Ther. Targets, 11 (2007) 363-373.

[10] M.R. Warr, G.C. Shore, Unique biology of Mcl-1: therapeutic opportunities in cancer, Curr. Mol. Med., 8 (2008) 138-147.

[11] S. Caenepeel, S.P. Brown, B. Belmontes, G. Moody, K.S. Keegan, D. Chui, D.A. Whittington, X. Huang, L. Poppe, A.C. Cheng, M. Cardozo, J. Houze, Y. Li, B. Lucas, N.A. Paras, X. Wang, J.P. Taygerly, M. Vimolratana, M. Zancanella, L. Zhu, E. Cajulis, T. Osgood, J. Sun, L. Damon, R.K. Egan, P. Greninger, J.D. McClanaghan, J. Gong, D. Moujalled, G. Pomilio, P. Beltran, C.H. Benes, A.W. Roberts, D.C. Huang, A. Wei, J. Canon, A. Coxon, P.E. Hughes, AMG 176, a Selective MCL1 Inhibitor, Is Effective in Hematologic Cancer Models Alone and in Combination with Established Therapies, Cancer Discov., 8 (2018) 1582-1597.

[12] X. Yi, A. Sarkar, G. Kismali, B. Aslan, M. Ayres, L.R. Iles, M.J. Keating, W.G. Wierda, J.P. Long, M.T.S. Bertilaccio, V. Gandhi, AMG-176, an Mcl-1 Antagonist, Shows Preclinical Efficacy in Chronic Lymphocytic Leukemia, Clin. Cancer. Res., 26 (2020) 3856-3867.

[13] A. Nencioni, F. Hua, C.P. Dillon, R. Yokoo, C. Scheiermann, M.H. Cardone, E. Barbieri, I. Rocco, A. Garuti, S. Wesselborg, C. Belka, P. Brossart, F. Patrone, A. Ballestrero, Evidence for a protective role of Mcl-1 in proteasome inhibitor-induced apoptosis, Blood, 105 (2005) 3255-3262.

[14] F. Morales, A. Giordano, Overview of CDK9 as a target in cancer research, Cell Cycle, 15 (2016) 519-527.

[15] T. Wu, Z. Qin, Y. Tian, J. Wang, C. Xu, Z. Li, J. Bian, Recent Developments in the Biology and Medicinal Chemistry of CDK9 Inhibitors: An Update, J. Med. Chem., (2020).

[16] D.C. Phillips, S. Jin, G.P. Gregory, Q. Zhang, J. Xue, X. Zhao, J. Chen, Y. Tong, H. Zhang, M. Smith, S.K. Tahir, R.F. Clark, T.D. Penning, J.R. Devlin, J. Shortt, E.D. Hsi, D.H. Albert, M. Konopleva, R.W. Johnstone, J.D. Leverson, A.J. Souers, A novel CDK9 inhibitor increases the efficacy of venetoclax (ABT-199) in multiple models of hematologic malignancies, Leukemia, 34 (2020) 1646-1657.

[17] D.A. Luedtke, Y. Su, J. Ma, X. Li, S.A. Buck, H. Edwards, L. Polin, J. Kushner, S.H. Dzinic, K. White, H. Lin, J.W. Taub, Y. Ge, Inhibition of CDK9 by voruciclib synergistically enhances cell death induced by the Bcl-2 selective inhibitor venetoclax in preclinical models of acute myeloid leukemia, Signal Transduct. Target. Ther., 5 (2020) 17.

[18] E. Walsby, G. Pratt, H. Shao, A.Y. Abbas, P.M. Fischer, T.D. Bradshaw, P. Brennan, C. Fegan, S. Wang, C. Pepper, A novel Cdk9 inhibitor preferentially targets tumor cells and synergizes with fludarabine, Oncotarget, 5 (2014) 375-385.

[19] M.H. Rahaman, Y. Yu, L. Zhong, J. Adams, F. Lam, P. Li, B. Noll, R. Milne, J. Peng, S. Wang, CDKI-73: an orally bioavailable and highly efficacious CDK9 inhibitor against acute myeloid leukemia, Invest. New Drugs, 37 (2019) 625-635.

[20] M.H. Rahaman, F. Lam, L. Zhong, T. Teo, J. Adams, M. Yu, R.W. Milne, C. Pepper, N.A. Lokman, C. Ricciardelli, M.K. Oehler, S. Wang, Targeting CDK9 for treatment of colorectal cancer, Mol. Oncol., 13 (2019) 2178-2193.

[21] S. Xie, H. Jiang, X.W. Zhai, F. Wei, S.D. Wang, J. Ding, Y. Chen, Antitumor action of CDK inhibitor LS-007 as a single agent and in combination with ABT-199 against human acute leukemia cells, Acta Pharmacol. Sin., 37 (2016) 1481-1489.

[22] H. McCalmont, K.L. Li, L. Jones, J. Toubia, S.C. Bray, D.A. Casolari, C. Mayoh, S.E. Samaraweera, I.D. Lewis, R.K. Prinjha, N. Smithers, S. Wang, R.B. Lock, R.J. D'Andrea, Efficacy of combined CDK9/BET inhibition in preclinical models of MLL-rearranged acute leukemia, Blood Adv., 4 (2020) 296-300.

[23] J. Li, X. Zhi, S. Chen, X. Shen, C. Chen, L. Yuan, J. Guo, D. Meng, M. Chen, L. Yao, CDK9 inhibitor CDKI-73 is synergetic lethal with PARP inhibitor olaparib in BRCA1 wide-type ovarian cancer, Am. J. Cancer Res., 10 (2020) 1140-1155.

[24] Y.A. Sonawane, M.A. Taylor, J.V. Napoleon, S. Rana, J.I. Contreras, A. Natarajan, Cyclin Dependent Kinase 9 Inhibitors for Cancer Therapy, J. Med. Chem., 59 (2016) 8667-8684.

[25] R. Chen, M.J. Keating, V. Gandhi, W. Plunkett, Transcription inhibition by flavopiridol: mechanism of chronic lymphocytic leukemia cell death, Blood, 106 (2005) 2513-2519.

[26] C.M. Olson, B. Jiang, M.A. Erb, Y. Liang, Z.M. Doctor, Z. Zhang, T. Zhang, N. Kwiatkowski, M. Boukhali, J.L. Green, W. Haas, T. Nomanbhoy, E.S. Fischer, R.A. Young, J.E. Bradner, G.E. Winter, N.S. Gray, Pharmacological perturbation of CDK9 using selective CDK9 inhibition or degradation, Nat Chem. Biol., 14 (2018) 163-170.

[27] B. Wang, J. Wu, Y. Wu, C. Chen, F. Zou, A. Wang, H. Wu, Z. Hu, Z. Jiang, Q. Liu, W. Wang, Y. Zhang, F. Liu, M. Zhao, J. Hu, T. Huang, J. Ge, L. Wang, T. Ren, Y. Wang, J. Liu, Q. Liu, Discovery of 4-(((4-(5-chloro-2-(((1s,4s)-4-((2-methoxyethyl)amino)cyclohexyl)amino)pyridin-4- yl)thiazol-2-yl)amino)methyl)tetrahydro-2H-pyran-4-carbonitrile (JSH-150) as a novel highly selective and potent CDK9 kinase inhibitor, Eur. J. Med. Chem., 158 (2018) 896-916.

[28] J. Cidado, S. Boiko, T. Proia, D. Ferguson, S.W. Criscione, M. San Martin, P. Pop-Damkov, N. Su, V.N. Roamio Franklin, C. Sekhar Reddy Chilamakuri, C.S. D'Santos, W. Shao, J.C. Saeh, R. Koch, D.M. Weinstock, M. Zinda, S.E. Fawell, L. Drew, AZD4573 Is a Highly Selective CDK9 Inhibitor That Suppresses MCL-1 and Induces Apoptosis in Hematologic Cancer Cells, Clin. Cancer Res., 26 (2020) 922-934.

[29] J. Xu, H. Li, X. Wang, J. Huang, S. Li, C. Liu, R. Dong, G. Zhu, C. Duan, F. Jiang, Y. Zhang, Y. Zhu, T. Zhang, Y. Chen, W. Tang, T. Lu, Discovery of coumarin derivatives as potent and selective cyclin-dependent kinase 9 (CDK9) inhibitors with high antitumour activity, Eur. J. Med. Chem., 200 (2020) 112424.

[30] H. Shao, S. Shi, S. Huang, A.J. Hole, A.Y. Abbas, S. Baumli, X. Liu, F. Lam, D.W. Foley, P.M. Fischer, M. Noble, J.A. Endicott, C. Pepper, S. Wang, Substituted 4-(thiazol-5-yl)-2-(phenylamino)pyrimidines are highly active CDK9 inhibitors: synthesis, X-ray crystal structures, structure-activity relationship, and anticancer activities, J. Med. Chem., 56 (2013) 640-659.

[31] H. Shao, S. Shi, D.W. Foley, F. Lam, A.Y. Abbas, X. Liu, S. Huang, X. Jiang, N. Baharin, P.M. Fischer, S. Wang, Synthesis, structure-activity relationship and biological evaluation of 2,4,5-trisubstituted pyrimidine CDK inhibitors as potential anti-tumour agents, Eur. J. Med. Chem., 70 (2013) 447-455.

[32] S. Grosjean, S. Triki, J.-C. Meslin, K. Julienne, D. Deniaud, Synthesis of nitrogen bicyclic scaffolds: pyrimido[1,2-a]pyrimidine-2,6-diones, Tetrahedron, 66 (2010) 9912-9924.

[33] A. Noack, H. Hartmann, Synthesis and characterisation of N,N-disubstituted 2-amino-5-acylthiophenes and 2-amino-5-acylthiazoles, Tetrahedron, 58 (2002) 2137-2146.

[34] R.J. Highet, W.C. Wildman, Solid Manganese Dioxide as an Oxidizing Agent, J. Am. Chem. Soc., 77 (1955) 4399-4401.

[35] S. Wang, C. Meades, G. Wood, A. Osnowski, S. Anderson, R. Yuill, M. Thomas, M. Mezna, W. Jackson, C. Midgley, G. Griffiths, I. Fleming, S. Green, I. McNae, S.Y. Wu, C. McInnes, D. Zheleva, M.D. Walkinshaw, P.M. Fischer, 2-Anilino-4-(thiazol-5-yl)pyrimidine CDK inhibitors: synthesis, SAR analysis, X-ray crystallography, and biological activity, J. Med. Chem., 47 (2004) 1662-1675.

[36] X. Huang, Y. He, Y. Ding, The Novel Syntheses of α-Trifluoromethylated Ketones from β-Bromoenol Phosphates, Phosphorus, Sulfur, Silicon Relat. Elem., 174 (2006) 201-207.

[37] V. Krystof, I. Chamrad, R. Jorda, J. Kohoutek, Pharmacological targeting of CDK9 in cardiac hypertrophy, Med. Res. Rev., 30 (2010) 646-666.

[38] T. Shimamura, J. Shibata, H. Kurihara, T. Mita, S. Otsuki, T. Sagara, H. Hirai, Y. Iwasawa, Identification of potent 5-pyrimidinyl-2-aminothiazole CDK4, 6 inhibitors with significant selectivity over CDK1, 2, 5, 7, and 9, Bioorg. Med. Chem. Lett., 16 (2006) 3751-3754.

[39] S. Ali, D.A. Heathcote, S.H. Kroll, A.S. Jogalekar, B. Scheiper, H. Patel, J. Brackow, A. Siwicka, M.J. Fuchter, M. Periyasamy, R.S. Tolhurst, S.K. Kanneganti, J.P. Snyder, D.C. Liotta, E.O. Aboagye, A.G. Barrett, R.C. Coombes, The development of a selective cyclin-dependent kinase inhibitor that shows antitumor activity, Cancer Res., 69 (2009) 6208-6215.

[40] S. Wang, G. Griffiths, C.A. Midgley, A.L. Barnett, M. Cooper, J. Grabarek, L. Ingram, W. Jackson, G. Kontopidis, S.J. McClue, C. McInnes, J. McLachlan, C. Meades, M. Mezna, I. Stuart, M.P. Thomas, D.I. Zheleva, D.P. Lane, R.C. Jackson, D.M. Glover, D.G. Blake, P.M. Fischer, Discovery and characterization of 2-anilino-4- (thiazol-5-yl)pyrimidine transcriptional CDK inhibitors as anticancer agents, Chem. Biol., 17 (2010) 1111-1121.

[41] C. McInnes, S. Wang, S. Anderson, J. O'Boyle, W. Jackson, G. Kontopidis, C. Meades, M. Mezna, M. Thomas, G. Wood, D.P. Lane, P.M. Fischer, Structural determinants of CDK4 inhibition and design of selective ATP competitive inhibitors, Chem. Biol., 11 (2004) 525-534.

[42] G.D. Diana, P. Rudewicz, D.C. Pevear, T.J. Nitz, S.C. Aldous, D.J. Aldous, D.T. Robinson, T. Draper, F.J. Dutko, C. Aldi, et al., Picornavirus inhibitors: trifluoromethyl substitution provides a global protective effect against hepatic metabolism, J. Med. Chem., 38 (1995) 1355-1371.

[43] R. Filler, R. Saha, Fluorine in medicinal chemistry: a century of progress and a 60-year retrospective of selected highlights, Future Med. Chem., 1 (2009) 777-791.

[44] F. Leroux, Atropisomerism, biphenyls, and fluorine: a comparison of rotational barriers and twist angles, Chembiochem, 5 (2004) 644-649.

[45] K. Muller, C. Faeh, F. Diederich, Fluorine in pharmaceuticals: looking beyond intuition, Science, 317 (2007) 1881-1886.

[46] V. Caracciolo, G. Laurenti, G. Romano, V. Carnevale, A.M. Cimini, C. Crozier-Fitzgerald, E. Gentile Warschauer, G. Russo, A. Giordano, Flavopiridol induces phosphorylation of AKT in a human glioblastoma cell line, in contrast to siRNA-mediated silencing of Cdk9: Implications for drug design and development, Cell Cycle, 11 (2012) 1202-1216.